applied sciences

MDPI

Review

The Use of Graphene and Its Derivatives for the Development of Polymer Matrix Composites by Stereolithographic 3D Printing

Ioana Chiulan [1,*], Ştefan Ioan Voicu [1,2] and Dan Batalu [3]

[1] Advanced Polymer Materials Group, University Politehnica of Bucharest, 1-7 Gh. Polizu Street, 011061 Bucharest, Romania; stefan.voicu@upb.ro
[2] Department of Analytical Chemistry and Environmental Engineering, Faculty of Applied Chemistry and Materials Science, University Politehnica of Bucharest, 1-7 Gh. Polizu Street, 011061 Bucharest, Romania
[3] Faculty of Materials Science and Engineering, University Politehnica of Bucharest, Splaiul Independentei 313, 060042 Bucharest, Romania; dan_batalu@yahoo.com
* Correspondence: ioana.chiulan@chimie.upb.ro or ioana.chiulan@yahoo.com

Abstract: Significant advances in graphene-based materials have facilitated the development of various composites structures in a diverse range of industry sectors. At present, the preparation of graphene-added materials is mainly developed through traditional methods. However, in recent years, additive manufacturing emerged as a promising approach that enables the printing of complex objects in a layer-by-layer fashion, without the need for moulds or machining equipment. This paper reviews the most recent reports on graphene-based photopolymerizable resins developed for stereolithography (SLA), with particular consideration for medical applications. The characteristics of the SLA technology, the most suitable raw materials and formulations and the properties of final 3D products are described. Throughout, a specific focus is placed on the mechanical properties and biocompatibility of the final 3D-printed object. Finally, remaining challenges and future directions are also discussed.

Keywords: 3D printing; stereolithography; graphene; polymer matrix composites

check for updates

Citation: Chiulan, I.; Voicu, Ş.I.; Batalu, D. The Use of Graphene and Its Derivatives for the Development of Polymer Matrix Composites by Stereolithographic 3D Printing. *Appl. Sci.* **2022**, *12*, 3521. https://doi.org/10.3390/app12073521

Academic Editor: Andrea Dorigato

Received: 2 March 2022
Accepted: 29 March 2022
Published: 30 March 2022

Publisher's Note: MDPI stays neutral with regard to jurisdictional claims in published maps and institutional affiliations.

Copyright: © 2022 by the authors. Licensee MDPI, Basel, Switzerland. This article is an open access article distributed under the terms and conditions of the Creative Commons Attribution (CC BY) license (https://creativecommons.org/licenses/by/4.0/).

1. Introduction

Nowadays, the fabrication at an industrial scale of items for healthcare occurs in an overwhelming proportion through conventional techniques. The simplicity and cost-effectiveness of the traditional manufacturing technologies make them suitable, especially for ready-to-use medical devices. This category includes devices made from thermoplastic polymers designed for ex vivo use in different medical procedures (valves, closures) or in vivo implantation (orthopaedic implants, catheters and others), which are prepared using hot-melt extrusion or injection moulding, thus are mass products [1]. However, the focus of recent fundamental research is to explore new manufacturing opportunities that address equally the needs for customizable products and for scalable technologies. With respect to regenerative medicine, the complexity of the 3D microenvironment, the relation between different cell types, and the interactions between cells and the extracellular matrix require different scientific tools to develop the proper human-like tissue or organs. For example, scaffolds intended to be used for tissue engineering are commonly developed through freeze-drying, salt leaching, electrospinning, and thermally induced phase separation [2]. However, there are some important drawbacks to these conventional techniques, such as their insufficient mechanical resistance for use in load-bearing applications, residual salt particles, small scale production, slow sublimation of the solvent, lack of control over scaffold topology [3]. In this context, additive manufacturing (AM) emerged as a group of techniques that allow fabricating 3D objects with controlled geometrical parameters

(pore shape and size, pore distribution, interconnections between pores) with superior repeatability and reproducibility.

Additive manufacturing involves the use of starting materials in the form of filaments, pellets, powders, liquid resins, ceramic pastes, gels to create solid objects of various architecture, from very small to very large dimensions. Common AM technologies used to fabricate healthcare devices or tools are Fused Deposition Modelling (FDM, coined as a trademark by Stratasys, also known as Extrusion Deposition, ED, or Material Extrusion, ME, or Fused Filament Fabrication, FFF), stereolithography (SLA), powder bed fusion (PBD), inkjet printing (IP) and others. Common for all the techniques is the use of digital models built up from scans of real-life objects or from computer-assisted design (CAD) models. Specialized software then converts the digital model into slices and finally into g-code files, usually which the machine prints layer-by-layer into 3D forms. AM was initially adopted by the companies in the automotive industry, but as the technology advanced, it was implemented in other fields, such as the medical sector, to reproduce anatomical parts through the data from image processing of the computer tomography scan file, implants or scaffolds.

The curing of liquid resins occurs as a result of thermal or light-activated polymerization and can be carefully controlled and optimized through temperature and irradiation conditions, respectively. The process of VAT polymerization, represented by SLA, digital light processing (DLP), continuous liquid interface production (CLIP) and two-photon polymerization (2PP), uses a laser as a light source to cure photopolymerizable resins. In SLA and DLP, the curing process occurs when using either UV light (365–385 nm) or visible light (405 nm), as in 2PP near-infrared (NIR), a laser beam (532 nm) is used [4]. These techniques ensure high printing resolution (25–100 µm, even 0.1–0.2 for 2PP) for the fabrication of precise items for dental reconstruction [5,6], delivery devices (microneedles for insulin skin delivery [7], implantable drug delivery system for osteosarcoma chemotherapy [8]) scaffolds for bone tissue engineering [9], microfluidics chips [10]. The main properties of VAT polymerization technologies have recently been reviewed in detail [11]. DLP technique uses a projector light source, and each entire layer is exposed all at once, which ensures a faster printing speed compared to SLA (where a UV laser beam is curing the layers line by line) and improves the efficiency. Drawback relies on the accuracy of the printed parts, which depends on the projector resolution. The CLIP technique was developed in 2015 and is up to 100 times faster than any other 3D printing method [12]. The fundamental concept is similar to that of DLP, excepting the use of an oxygen-permeable window instead of a glass window. This is responsible for the creation of a "dead zone" between the window and the printed part, where photopolymerization is inhibited and a very thin layer of resin remains uncured. As a result, the resolution of the printed object increases and the risk of printing failure due to peeling forces decreases [11]. Two-photon polymerization uses the two-photon absorption of NIR light to excite the photoinitiator in a monomer solution at the focal spot only, initiating the polymerization in a very small volume called "voxel" [13]. By using this technology, the material is no longer deposited in a "layer-by-layer" manner, and the fabrication of complex 3D microstructures becomes possible. Unfortunately, the toxicity of many feedstock materials limits the use of 2PP for biological applications [14]. Moreover, the equipment is much more expensive than others based on photopolymerization. Herein, attention is paid to SLA technology, for its excellent abilities to print complex 3D ceramic (based on special composite resins and heat treatment postprocessing) and polymer structures, for biomedical field with high accuracy, high printing speed and low costs. In particular, SLA has been already applied to fabricate 3D structured graphene-based polymer composites.

The materials suitable for 3D printing have to feature facile processability and stability during storage, along with cost-effectiveness and abundance of the raw materials required for industrial demands. Materials for SLA are clear resins, resins with additives and resins with added nano/micro functional particles. In general, the addition of fillers in the SLA resin leads to a stiffer and stronger fabricated structure than additive-free polymer resin.

Except for the mechanical properties' improvement, electrical conductivity can be achieved by the addition of carbon-based nanofillers, such as carbon nanotubes, carbon nanofiber, carbon-black, and graphene have been added to fabricate composites [15].

The graphene family is considered an important nanofillers as it increases the stiffness, conductivity [16] and, in some cases, cytocompatibility. Graphene and its derivatives represent the central point for a wide range of applications and technical solutions. Though they were initially used as filler in composite polymeric materials due to their high surface area and excellent mechanical properties [17–20], more and more applications started to also value the high electrical conductivity or potential of these species for separative or other advanced applications. In the field of sensors and biosensors, graphene is one of the most important candidates. With a high ability for adsorbing, even gas molecules can be used with minimum manufacturing stages for obtaining industrial sensors [21,22]. Energy storage devices based on graphene can be obtained under a wide range of products such as fuel cells, batteries or even solar cells [23]. One of the most fascinating fields for electronic applications is represented by the biosensors due to the high versatility for functionalization reactions and the possibility to immobilize surface enzymes, proteins or other active biological chemical species and thus, the potential uses are practical unlimited [24]. In the field of environmental protection, the adsorption of metal oxides can lead to a lot of catalysis applications for the degradation of organic substances from water [25] or directly for water filtration through composite membranes with graphene, in which the filler act as a molecular sieve [26]. Latest applications in the medical field include tissue engineering for bone repair by favouriting osteogenesis [27], soft tissues regeneration by active behaviour in cells differentiation, direct or via functionalization [28], or even haemodialysis using composite membranes with functionalized graphene for removal of heavy metal ions from blood in case of intoxications [29–31]. Unfortunately, incorporating graphene and graphene oxide increases the opacity of the prepolymer solution, which absorbs more UV light and subsequently decreases photoinitiator conversion, and longer exposure time and/or higher power light sources are required. Consequently, this may compromise the cell viability in the bioprinted system. In addition, the solution become too opaque at higher nanofiller concentration to ensure a good printing quality. The graphene processability is still considered as a technical obstacle to its widespread uptake by industry. Another important limitation is the brittleness of the 3D outputs made of graphene-based materials due to graphene's defects such as vacancies, grain beads and dislocations, that may cause fractures when subjected to stress [32]

In the literature, numerous recent reviews concerning the applications of 3D-printed graphene nanocomposites can be found [33–36]. However, the research work concerning the use of graphene and bio-based UV curable materials for regenerative medicine and biomedical devices developed for SLA is scarcely represented. Therefore, the aim of this work is to present in a concise manner the current state-of-the-art on graphene-based materials, with a special focus on the biomaterials printed through stereolithography.

2. Overview of the Conventional Techniques for Graphene-Added Biomaterials

At present, the preparation of graphene-added materials are mainly developed through melt blending [37], electrospinning [38], solvent-assisted casting technique [39–41], in situ polymerization [42,43], layer-by-layer assembly [44,45], freeze-drying [46]. Unfortunately, the full potential of using graphene in a polymer matrix is not reached due to its aggregation. Moreover, the absence of active groups on the graphene surface weakens the forces between the polymer matrix and graphene; hence, phase separation occurs.

Melt processing was embraced by the industry for obvious reasons: it is cost-effective, simple and facilitates large scale production for a wide range of affordable products. The process consists in melting the polymer pellets and mixing them with fillers and additives by applying a high shear force for homogeneity. Clearly, the uselessness of using solvents to disperse the filler into the polymer matrix is an advantage for environmental and safety reasons since organic solvents are toxic. Though, the downsides of this technique

are: (i) the poor dispersion of the filler in the polymer matrix, specifically in higher filler loadings due to the high viscosity of the mixture [47,48], (ii) requires high temperature to ensure the homogeneity of the mixture, which can cause occasional degradation of the polymer, and (iii) works preferentially with thermoplastics (polyethene, polypropylene, polyethene terephthalate, polyvinylchloride, polyamides, polycarbonates, polyurethanes and silicones).

In terms of medical applications, the first option is the use of biopolymers as matrices, as they can replace parts of soft and hard tissue and their degradation products are not immunogenic. Secondly, the environmental problems related to fossil-based polymers moved the attention to the synthesis of polymers starting from raw materials that can be obtained from renewable resources (e.g., starch, glucose, cellulose resulting from bacterial fermentation). Such an example is poly(butylene succinate), which exhibits mechanical and thermal properties comparable with polyethene and polypropylene. Platnieks et al. [49] reported the melt blending of poly(butylene succinate) with graphene nanoplatelets in a concentration from 0.5 to 6.0 wt%. Importantly, graphene nanoplatelets were found to increase the thermal conductivity during melt blending of poly(butylene succinate), which facilitate the reduction of the processing parameters, i.e., temperature and time, and thus the thermal degradation of the thermoplastic biopolymer can be prevented. The melt processing technology is inappropriate for many biopolymers currently used in tissue engineering, such as proteins or other natural polymers. Apart from that, the complexity of the final shapes is reduced, and, most importantly, the high processing temperature hinders the survival of the embedded cells.

Solution blending is another extensive method for the preparation of graphene/polymer composites, mainly due to its accessibility. The process consists of the dispersion of graphene in an organic solvent under sonication, followed by the addition of the polymer, and, finally, removing the solvent. In this process, an important issue is the difficulty of uniformly dispersing graphene in the polymer solution. To overcome this, scientists have several choices: the addition of complex dispersing agents [50], graphene functionalization [51] or synthesis of chemically reduced GO (r-GO) in the presence of NaCl, which acts as a flocculant and simplifies the redispersion of r-GO aggregates in organic media [52]. However, the most important shortcoming of the solvent blending method relates exactly to the use of organic solvents, which are adsorbed between the graphene layers and cannot be completely removed, even at high temperatures [53]. In the end, this affects the performances of the final composites.

The electrospinning technique is a versatile method to realize uniform dispersion, as well as the effective alignment of fillers [54]. Subsequent hot pressing of the aligned electrospun fibres led to the fabrication of polymer composites with enhanced mechanical properties. Electrospinning has several limitations in the preparation of graphene-based materials, including the limited variety of polymers that can be used, friability of the graphene fibres after calcination, high production cost when implemented at the industrial level [55].

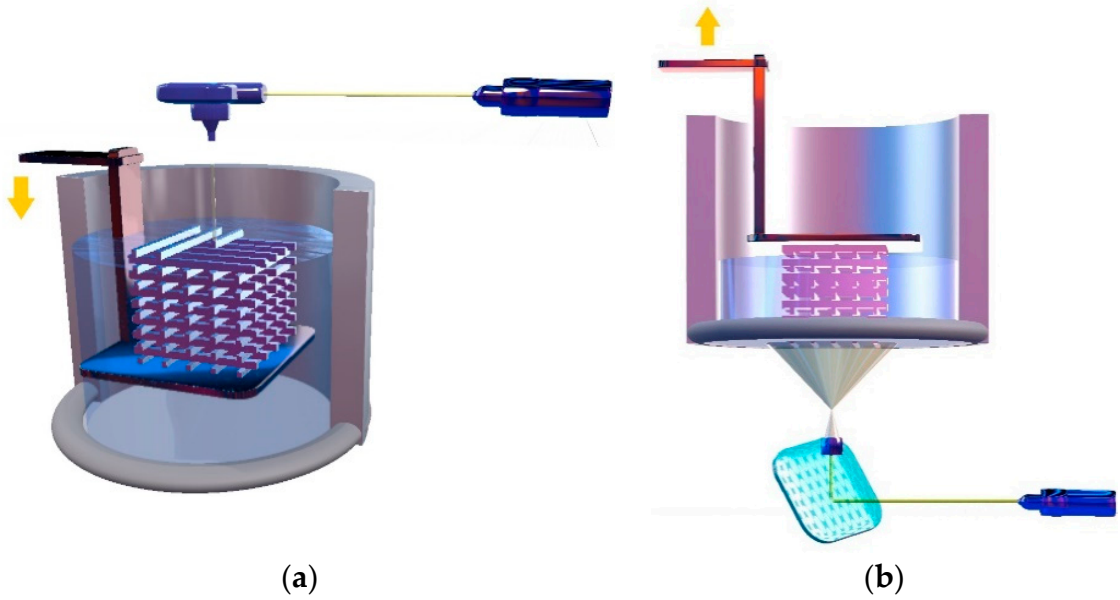
Alternatively, in situ polymerization is widely used in the synthesis of graphene-reinforced composites due to its benefit in improving their mechanical, electrical and thermal properties [56]. The reasons for this include the low amounts of organic solvents, the higher dispersion of the filler in the polymer matrix and enhanced graphene-polymer interactions. Moreover, polymer composites with high filler content can be prepared. Basically, this technique consists in blending the graphene or graphene derivative with a monomer or prepolymer, then adding the suitable initiator. The reaction occurs upon irradiation or heating conditions.

More recently, Dalai and Sreekanth [57] reported the fabrication of graphene reinforced ultra-high molecular weight polyethene nanocomposite by combining the process of ball milling with compression moulding. The high values of flexural strength and flexural modulus recommend the composite with 0.5 wt% of graphene loaded as a material suitable for total joint replacement.

3. Stereolithography: Top-Down and Bottom-Up Approaches

Stereolithography was patented in 1986 by Chuck Hull (US Patent 4,575,330), and the first SLA printers were developed by 3D Systems [58]. It is the first commercially available AM technique, opening the door to a new era in manufacturing. An SLA apparatus is equipped with a laser source usually emitting light in the UV range that is directed by means of lenses to a reservoir filled with a liquid photocurable resin. The light beam is controlled in an XY direction, and a fabrication platform allows vertical movement. Depending on the orientation of the laser and the surface of the photopolymerization occurs, SLA may have two kinds of configurations: (i) top-down and (ii) bottom-up [59,60].

In the top-down process, the resin vat is exposed to the laser beam from the top (Figure 1a). When the curing of the first layer is completed, the building platform is moved downward along the *Z*-axis, exposing the second layer of the resin to irradiation. The thickness of the printed layer through this technique can be controlled by the intensity of the light source, scanning speed, depth of focus, and exposure time [61]. The printing quality depends on the irradiating parameters (power, speed, laser source), resin chemical composition and operation settings (speed, orientation). Specific drawback refers to the height of the 3D-printed objects, which is limited by the vat depth, as the objects are fabricated facing upward [59]. A larger vat means that more resin is needed and, consequently, the amount of the resin waste rises. Moreover, the printing efficiency in this configuration is reduced due to the extra time needed to level the resin's surface, which is disturbed when the platform moves. Finally, the contact of the cured layers with atmospheric oxygen limits the crosslinking efficiency [61].



(**a**) (**b**)

Figure 1. Schematic illustration of SLA approaches: (**a**) top-down; (**b**) bottom-up.

In the bottom-up orientation (Figure 1b), the fabrication platform is dipped into the resin vat, whose bottom surface is transparent and non-adhering. The light is projected from underneath, initiating the photopolymerization of the resin film between the movable platform and the bottom of the vat. After the curing of the first layer, the platform moves up, and photopolymerization continues with a new layer, which is fabricated underneath the previous one. This technique allows the printing of high objects with the use of low resin volumes [61]. Additionally, the cured layers are not exposed to the atmosphere, so the inhibition of the photopolymerization reaction is prevented. Specific advantages of bottom-up techniques refer to smaller layer thickness, which can be accurately controlled by the elevator, higher vertical resolution and surface quality [59,62]. The common SLA 3D printer models are manufactured by Formlabs, 3D Systems, Full Spectrum Laser, Asiga, etc.

SLA is applicable for prototypes of scaffolds for tissue engineering or regenerative medicine that can be fabricated rapidly and with high feature resolution (5–50 µm).

4. Materials for SLA

SLA operates with liquid, thermoset photopolymers, which are mostly acrylates or epoxy resins. The composition of the photopolymer resin formulation has an important role in defining the curing behaviour. When used without fillers, photopolymers can produce minimum cure depths (i.e., the maximum depth that the laser power allows to cure on a single layer) between 25 and 100 µm [63]. The addition of fillers (pigments, ceramic powders or fibres) changes the curing behaviour in a complex manner, depending on the filler fraction, size, shape, and optical property. The accuracy of the SLA printing depends on the fibre length. The long fibres or aggregates of short fibres creates opacity against 355–405 nm irradiation and decreases the cure depth, which consequently leads to additional post-processing of the printed objects [64].

4.1. Resins

The process of photopolymerization requires the presence of three major components: the resin, the photoinitiator and the light source. The most important ingredient used in SLA printing is resin. The photocurable resins are multifunctional monomers and oligomers, typically from the class of (meth)acrylates, epoxides and thiol-enes [65]. The acrylic resins undergo photopolymerization through a radical mechanism. When exposed to UV light, the photoinitiators produce free radicals that attack the double bond of the (meth)acrylic monomers, which subsequently transfer the radical to another monomer, and the polymer chain grows. In contrast to acrylates and methacrylate, epoxy monomers are polymerized through an ionic mechanism. In this case, the cationic photoinitiators produce acids that react with a bond in epoxy monomers and induce polymerization. Some commercial epoxy monomers used in SLA are bisphenol A diglycidyl ether (DGEBA) or 3,4-epoxycyclohexylmethyl-3,4-epoxycyclohexane carboxylate (ECC) [66]. Those liquid monomers/oligomers are converted into a solid polymer within seconds or a few minutes. The polymerization is initiated by active species (e.g., free radicals or cations), formed when a photoinitiator decompose in the presence of UV (200–400 nm), visible (400–700 nm) and, more rarely, IR (700–1000 nm) light [65].

Other components can be added in low concentrations to the photocurable formulation to improve parameters for printability or the properties of the resin. For instance, diluents (e.g., trimethylolpropane triacrylate, dipropylene glycol diacrylate, monofunctional urethane acrylate) are used to reduce the viscosity of the printing resin, photo-absorbers are useful to control the penetration depth of the incident light, inert dyes can provide specific colours, and inhibitors help to prevent the premature polymerization of the acrylate-based resins [60]. Moreover, the addition of dispersion agents improves the tinctorial strength, reduces the resin viscosity and surface tension and prevent sedimentation of particles, while stabilizers enhance shelf-life stability during resin storage and maintain a stable viscosity. Finally, the incorporation of fillers confers improved the mechanical properties of the printed object. Most often, the exact composition of a commercial resin is not publicly disclosed.

Synthetic polymers are by far the most used resin for SLA, as they are affordable, highly versatile and possess a very good light sensitiveness. Materials traders such as 3D Systems, FormLabs, etc., provide a wide range of acrylic, epoxy, vinyl ether photopolymers, polycarbonate-like, acrylonitrile-butadiene-styrene (ABS)-like and polypropylene-like materials. Notably, commercialized photopolymer resins are predominantly fossil-based and relatively expensive. Resins for SLA are continuously developed, making them useful for more-demanding biodegradable, human safety, and environmentally friendly products. Most of the available stereolithography resins form highly crosslinked networks, and the resulting materials are glassy or rigid. It should be noted that the focus is not on obtaining

a crosslinking density as higher as possible, which may lead to a brittle structure. For medical purposes, it is often necessary to develop objects with elastomer properties [67].

Biodegradable oligomers appropriate for SLA contain hydrolysable ester- or carbonate linkages in the main chain and contain molecules of D,L-lactide (DLLA), poly(propylenefumarate) (PPF), trimethylene carbonate (TMC) and ε-caprolactone (CL). The viscosity and glass transition of the macromers are key elements for prototyping and dictates the formulation of resin. Macromers of high molecular weight such as DLLA or PPF is diluted with non-reactive diluents such as N-methylpyrrolidone or water. Importantly, while curing, the material suffers an isotropic shrinkage, which should be taken into consideration when designing the prototype.

Despite this prevalence of petroleum-based resins for SLA printing, a progressive increase in the use of natural polymers from renewable resources can be noticed. Naturally derived oligomers bearing hydroxyl groups can be converted into photocurable resins through a simple chemical functionalization with methacrylic acid, glycidyl methacrylate and methacrylic anhydride. Most promising is the functionalization of natural polymers such as gelatin, alginate, oligopeptides that enable photocuring. Typically, this reaction occurs in phosphate-buffered saline solution by lightly heating (usually at 50 °C) a mixture of polymer and functionalization agent (4–5%). Specifically, gelatin, which is a major component of extracellular matrix (ECM) derived from the hydrolysis of collagen, is functionalized with methacrylate groups (GelMA) to form a matrix by photocrosslinking (Table 1). However, GelMA has relatively poor printability. Synthetic materials, most frequently belonging to the class of PEG derivatives, are frequently added to bio-resins based on natural polymers in order to modulate their mechanical properties, crosslinking or printability. For example, poly(ethylene glycol) diacrylate (PEGDA) was shown to enhance the printability and feature resolution of GelMA resin [68]. In another study, poly(ε-caprolactone) methacrylate was introduced into GelMA resin to improve the 3D printing fidelity and provided the hybrid materials with enhanced swelling and proliferation of seeded cells [69].

The utilization of plant oil polymers (polyesters, polyolefins, polyurethanes) in photoactive resin formulations for SLA is rarely reported so far. Vegetable oils contain fatty acids bearing large amounts of unsaturated bonds, which can be chemically modified with photocurable groups with epoxides, acrylates and methacrylates. Miao and co-workers [70] fabricated for the first time 4D scaffolds using epoxidized soybean oil acrylate (ESOA). The printed scaffolds could produce a shape recovery transition, determined by the oscillation of the pendant alkane groups present in the stearic, oleic and linoleic acids, the major fatty acids residues in the soybean oil. Epoxidized soybean oil acrylate has excellent biocompatibility and superior processing compared to PLA- and/or PCL-based liquid resin for stereolithography. Importantly, the printing speed and laser frequency have a significant influence on the thickness and width of the printed scaffold (Figure 2).

In another study, renewable ESOA-containing resin was developed to create biodegradable structures with similar mechanical properties to non-degradable commercial resins [71]. The mixture was composed of diluent (isobornyl methacrylate), oligomer (trifunctional epoxidized soybean oil acrylate, $ESOA_3$, difunctional/trifunctional epoxidized soybean oil methacrylate, $ESOMA_2$/$ESOMA_3$) and photoinitiator (phenylbis-2,4,6-trimethylbenzoyl phosphine oxide). Trifunctional epoxidized soybean oil methacrylate (Figure 3a) was synthesized via a "green" solvent-free synthesis route and demonstrated good layer fusion upon 3D printing (Figure 3b). The resulting polymers showed mechanical performance competitive to commercial counterparts. Other notable work on ESOA-based formulations for SLA 3D printing has been made [72,73], and the key findings from those studies are reported in Table 1.

Other vegetable oils, such as linseed oil, castor oil and cardanol oil, possesses inherent biodegradability, negligible toxicity and modifiable functional groups and are potential starting materials for the preparation of resins for 3D printing [74–76].

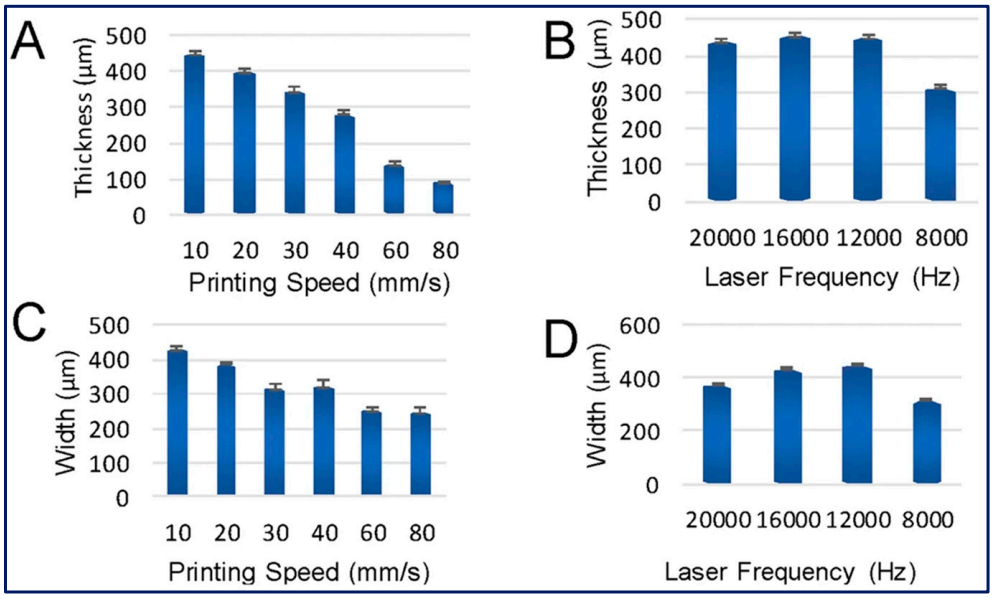


Figure 2. The effects of printing speed and laser frequency on printed scaffolds. (**A**) The effect of various printing speeds on thickness of struts at a laser frequency of 12,000 Hz. (**B**) The effect of various laser frequencies on thickness of struts at a printing speed of 10 mm/s. (**C**) The effect of various printing speeds on width of struts at a laser frequency of 12,000 Hz. (**D**) The effect of various laser frequencies on width of struts at a printing speed of 10 mm/s. Reprinted with permission from [70].

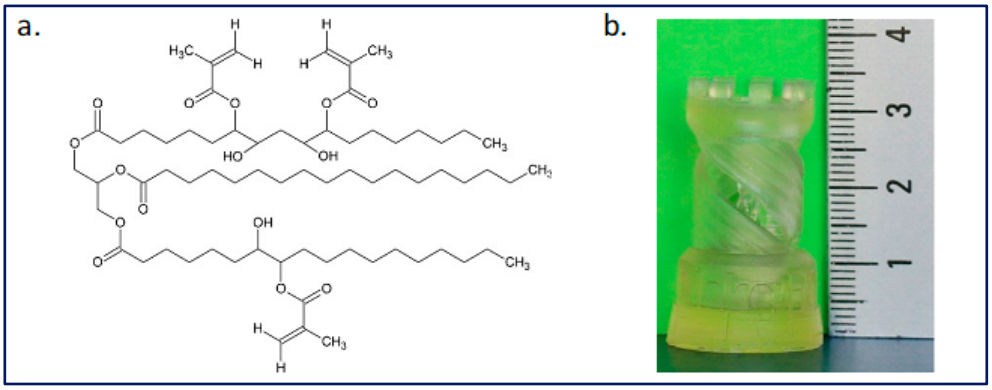


Figure 3. (**a**) Photocurable resin based on soybean oil for stereolithographic 3D printing and (**b**) picture of rook tower prototype printed with $ESOMA_3$. Reprinted with permission from [71].

The use of multiple resins for a printed object is possible by SLA, but it requires supplementary steps such as removal of unpolymerized resin, cleaning of the platform and partially fabricated object and resin change [61]. If these steps are performed manually, the cellular and biochemical purity may be compromised, but the automatic process has been recently explored [77].

Cell-containing structures were successfully prepared by SLA. In this technique, the resin is not subjected to shear stresses, unlike in nozzle-based technologies, and, thus, cell apoptosis is minimized during the printing of cell-laden biomaterials. Current research demonstrates the efficiency of the SLA printing process to manufacture objects with good structural integrity and complex design, suitable for the construction of different cell-laden structures.

Table 1. The representative resin for SLA 3D printing, suitable for biomedical applications.

Type of Resin	Functionality	Other Ingredients	Printing Conditions	Properties of the Printed Structure	Ref.
Gelatin	Methacrylamide	0.5% Irgacure 2959; neural stem cells (density of 2×10^6 cell/mL); graphene (1 mg/mL)	Sterile atmosphere, UV light	Homogeneous distribution of cells in the 3D-printed scaffold; well-defined architecture of the bioprinted hydrogels	[78]
Gelatin	Methacrylamide	0.5% Irgacure 2959; PEGDA (20%); graphene oxide (0, 0.05, 0.1, 0.25, 0.5 and 1 mg/mL)	200 µm diameter laser beam, 25 µJ intensity output of 20 kHz emitted UV, and 10 mm/s printing speed	GO improved mesenchymal stem cells adhesion on the surface of the scaffold and favored cell proliferation and differentiation;	[68]
Soybean oil	Acrylate	Irgacure 819	UV laser (355 nm), print speed between 10 to 80 mm/s, laser frequency from 8000 to 20,000 Hz	The layer thickness and width decreased dramatically with the increase in print speed, but slightly increased with increasing laser frequency. The compression modulus is not affected by differences in laser frequency. High attachment and proliferation of hMSCs	[70]
Soybean oil	Acrylate, di/trifunctional methacrylate	Isobornyl methacrylate, BAPO (1% *w*/*w*)	Halogen lamp (λ = 390−450 nm); post-curing in an UV oven (λ = 405 nm, 39 W) for 30 min at 60 °C; layer thickness of 100 µm	The functionality and the number of functional groups per oligomer tunes the stiffness and toughness of 3D products. Specifically, $ESOMA_3$ provides more stiffness and tensile strength than $ESOA_3$ and $ESOMA_2$ photoresins.	[71]
Soybean oil	Acrylate epoxidized	Photoinitiators: BAPO (0.25, 0.5, 1, and 2% *w*/*w*), TPO [(a)] (1% *w*/*w*), TPO-L [(b)]. Diluents: ethyl lactate, Genomer 1122TF	The resins were printed using Formlabs Form 2 printer under default settings	Increasing the ratio of BAPO in the resin significantly reduced the minimal exposure duration and the light penetration depth for the mixture. Custom made ESOA-based resins can be easily prepared with specific rheological and optical properties by adding diluents and PIs	[72]
Soybean oil	Acrylate epoxidized	Monomers used as reactive diluents: 1,6-hexanediol diacrylate (HDDA) and trimethylolpropane triacrylate (TMPTA). Photoinitiator: TPO (1%, 3%, 5%, and 7%)	UV-LED strips (λ = 405 nm); maximum power of 52.8 W. Irradiation time: 35 s for first 10 layers and 7.5 s for consecutive layers. Layer height: 0.5 mm.	Complete layer fusion; high-resolution features and good mechanical properties of the 3D-printed objects. The addition of the reactive diluents improved the mechanical properties.	[73]

[(a)] diphenyl(2,4,6-trimethylbenzoyl)phosphine oxide; [(b)] ethyl(2,4,6-trimethylbenzoyl) phenylphosphinate.

4.2. Graphene Composites

4.2.1. Overview of Graphene

Graphene is a nanomaterial consisting of ultra-thin sheets of sp^2 carbon atoms arranged in a honeycomb lattice structure, well known for its electronic, magneto-electronic and optoelectronic properties [79]. It was isolated from bulk graphite using mechanical exfoliation (via the "Scotch-tape" technique) [80], which is not a method suitable for mass-

scale production. The method developed by William Hummers in the late 1950s consists of the treatment of commercial graphite powder with oxidizing agents and strong acids [81]. The resulted material is actually graphene oxide, which can be further reduced through thermal [82] or chemical [83] methods, creating the so-called reduced graphene-oxide (rGO). Probably the most effective reductant is hydrazine [84], but its toxicity to humans and the environment boosted the scientists to find greener alternatives [85]. Other graphene production methods refer to ion implantation [86,87], liquid-phase exfoliation [88,89], epitaxial growth upon a silicon carbide substrate [90,91] and, the most significant chemical vapor deposition (CVD) [92–94]. Another important member of the graphene family is graphene quantum dots (GQDs), which are graphene sheets with a lateral dimension of <100 nm, but its potential is not consistently exploited in AM techniques yet. For in-depth details on the synthesis strategies and physical properties of graphene and its derivatives, we suggest some reviews for interested readers to refer to in the references [24,95–97].

Graphene is the nanofiller of choice due to its layered structural fillers having a large surface area (up to 2630 m^2/g) [98]. This is beneficial for obtaining high-performance composites as well as for loading drugs/biomolecules and brings the possibility of conjugating fluorescent dyes for bioimaging. Graphene reinforcement in AM offers a large spectrum of complex functional materials as a result of its inherent properties. However, the polymer matrix exhibits low dispersion efficiency, and therefore functionalization of graphene is required. In the oxidized form, the hydrophilic functional groups ensure a superior dispersion in an aqueous solution, increasing the accuracy and efficiency of the printing. Conversely, the graphene derivatives (GO, rGO, GQDS) offer a good dispersibility in polymer matrices and, for this reason, were selected as fillers in many polymer nanocomposite materials. GO stands out from this panel due to its unique hydrophilic, thermal, and electrical properties with high potential in medical science in stimuli-responsive materials [99–102], antibacterial materials [103], membranes in wound dressings [104], tissue-engineering scaffolds [105]. GO shows promising antimicrobial activity against Gram-positive and Gram-negative bacteria, phytopathogens and biofilm-forming microorganisms [106].

The functional groups of graphene derivatives (carboxyl, epoxide, hydroxyl) result in higher surface energy and superior compatibility with polar polymer matrices, often used for healthcare products. The study of graphene derivative bioinks is a growing field. The electrical properties of graphene are advantageous for developing complex cell-laden scaffolds for neural tissue engineering. Loaded neural stem cells in the GelMA/graphene bioink (G-GelMA) had differentiated and showed neurites elongation within the printed scaffold after two weeks of culture [78]. The printed hydrogel showed well-defined architecture, with a homogeneous distribution of the neural cells. Other authors used graphene oxide as an inorganic delivery carrier for nanoscale molecule drugs to develop a 3D scaffold for cartilage tissue engineering. A collagen-chitosan hydrogel was mixed with GO nanoparticles loaded with bone morphogenetic protein 7 (BMP7) and bioprinted into a structure that successfully reproduced the microenvironment of native cartilage [107].

GO, one of the most common derivatives of graphene, has been used in additive manufacturing in solid- or liquid-like formulations. For example, composite filaments with thermoplastic polymers such as ABS and PLA [108] were printed using a fused deposition technique and pastes made with water, and different materials (polyvinyl alcohol, ceramic powders such as SiC and Al_2O_3 and steel microspheres) were processed using robocasting [109]. The development of GO-based printing inks with high printability and biocompatibility is a major goal for 3D printing methods. Among the printing methods, stereolithography has emerged as a powerful tool to prepare structures with good resolution and high mechanical properties; therefore, the next section presents the graphene-based resin exclusively for SLA.

4.2.2. Three-Dimensional SLA Printing of Graphene and GO

At the academic level, graphene has been used as reinforcement in several photopolymer resins for a variety of applications, spanning from the development of semiconductors

to medical devices (Table 2). The properties of 3D printing are largely dependent on the dispersion of nanofillers. Generally, there are two main approaches to disperse graphene or GO in photocurable resins: directly in the liquid monomer, followed by the addition of initiators, or using a three-step method: (1) ultrasonication of a graphene/GO suspension in different solvents (acetone, chloroform, water, dimethyl formamide), (2) addition of polymer, and (3) removal of the solvent.

In tuning the properties of 3D-printed nanocomposite, the design of the resin should consider the aspect ratio and surface chemistry of the nanofiller, percolation threshold, and interfacial property of nanofiller and matrix. Often, in carbon-reinforced polymer composites, the addition of the nanofiller results in stronger but more brittle materials. In these cases, the reinforcement effect of increased tensile strength is overshadowed by a decrease in ductility, which leads to concerns about the toughness of the composite. Scientists followed two approaches to attain a more balanced strength/ductility relation, and these are the post-curing of 3D-printed parts and functionalizing GO.

Some examples are the works of Lin et al. [110] and Manapat et al. [111], who incorporated GO into SLA resin intended for 3D printing. Specimens with only 0.2 wt% GO showed a 62.2% increase in tensile strength without compromising ductility [110]. Furthermore, annealing the composite at 60 °C for 6 h and at 110 °C for another 6 h led to an increase of 12.8% in elongation compared with the uncured polymer matrix. The authors stated that this increase in ductility is due to the increasing crystallinity of GOs reinforced polymers. Manapat et al. observed an increase in ductility by about 15% at 0.5 wt% GO, but tensile strength decreased by 52% with further addition of GO [111]. Thus, 3D-printed specimens were annealed at 100 °C, and a drastic increase in strength by 673.6% for the 1 wt% GO nanocomposite was noticed (Figure 4a–c). However, the material became more brittle, showing a decrease in ductility by 82%. It is noteworthy that thermal post-curing facilitated the chemical crosslinking via esterification and decreasing in pore size of the resin, which explains the enhancement in mechanical strength. All these studies pointed out two important research directions in developing successful GO/photopolymers, namely the uniform GO dispersion in SLA resins and annealing treatment. In a recent example, Xiao et al. used mild annealing conditions on the SLA printed fibre-graphene oxide polymer composite resin designed for the development of new mechanical metamaterials [112]. After annealing, an enhancement in compression strength of almost 10 times, as compared with pure polymer, was obtained at a reinforcement content of 0.8 wt%.

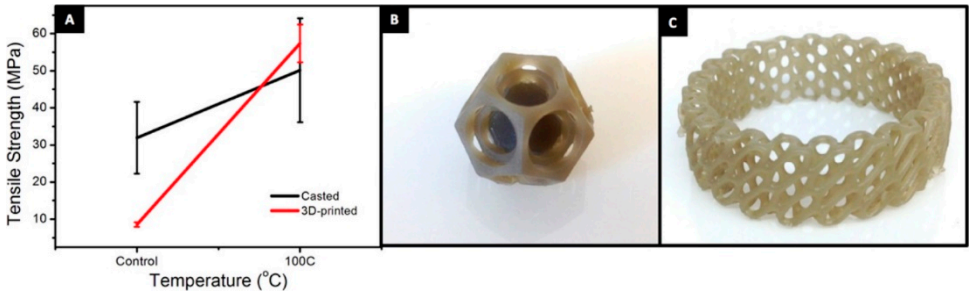


Figure 4. (**A**) Tensile strength comparison of casted and 3D-printed part. SLA-printed complex-shaped GO nanocomposites: (**B**) nested dodecahedron and (**C**) diagrid ring. Reprinted with permission from [111].

In 2019, Tsang et al. [113] explored for the first time the SLA technique as a likely way for the development of the GO/elastomer nanocomposites. The 3D-printed samples showed a decrease in mechanical and thermal properties with the addition of GO in the resin as a result of the filler agglomeration.

Overall, the literature on GO-reinforced polymers prepared via SLA is scarce, but graphene-based photopolymer resins are even less studied. The reason for this is the poor dispersion of graphene in the polymer matrix due to the lack of functional groups on

its surface. In the work of Lim et al., Tween20 was added to improve the dispersion of graphene into a graphene/photopolymer resin. The 3D-printed specimens exhibited a drop in tensile strength with the addition of graphene (1 and 2 wt%) as compared with pristine resin. The authors explained that the penetration of light is blocked by graphene, preventing complete crosslinking of the photopolymer resin [114,115]. The sample consisting of 2 wt% graphene had a rougher surface, with an appearance of bonded sand particles. Therefore, a low graphene content, less than 5 wt% according to some authors [116], is recommended to maintain the appearance and mechanical strength of the printed object. In the report of Wang et al. [116], a very small amount of graphene powder (0.1–2 wt‰) was doped into a 3D photocurable clear resin that could act as an inherent laser absorber and ionization promoter, which resulted in the direct analysis of samples without adding matrix for functional spectrometry devices.

An extra solvent can be added to disperse graphene, but in this case, the photocuring behaviour will be changed. In the work of Feng et al. [117], a solvent-free method was applied to fabricate scaffolds for bone tissue engineering. The UV-crosslinkable resin consisting of polylactic acid–polyurethane oligomer, trimethylolpropane trimethacrylate as a reactive diluent, Irgacure 819 and graphene was 3D printed, resulting in nanocomposites with better mechanical properties than commercial resins. Additionally, combining graphene with nanocellulose and incorporating it into UV-curable polyurethane (PU) has proven to impart new hybrid nanomaterials suitable for 3D printing [118]. The versatility of using graphene-PU resin in stereolithography has been explored by Ibrahim et al. [119]. The authors report that mixing graphene nanoplates with lignin results in strong interfacial interaction between functional groups of the lignin graphene and PU, and thus an enhanced filler-matrix compatibility. The tensile strength and hardness of the photocured PU composite increased significantly with a loading of 0.6 wt% lignin graphene.

Korhonen et al. [120] used GO reinforced commercial resin and fabricated 3D-printed structures via SLA. The samples were pyrolyzed under a nitrogen atmosphere to reduce GO to graphene and to decompose the polymer, resulting in 3D structures consisting entirely of graphene. Unfortunately, the graphene-based 3D structures showed high shrinking and brittleness, making them useless for practical applications.

Table 2. The representative 3D-printed graphene/GO-based composites.

Filler	Polymer Matrix	Resin Preparation	3D Printing Conditions	Post-Processing Steps	Applications	Ref.
Single-layer GO (SLGO)	Commercial polymer resin (Pic 100 from EnvisionTEC Inc., Dearborn, MI, USA)	SLGO was dispersed in acetone and ultrasonicated for 2 h; addition of polymer and ultrasonication for another 2 h; acetone evaporation by heating at 70 °C for 12 h; 0.2 and 0.5 wt% SLGO	3D printing was performed using a bottom-up mask projection-based SLA system	60 °C for 6 h and 110 °C for another 6 h	- [a]	[110]
GO prepared from graphite flakes using a modified Hummers method	Gray resin (FLGPGRO2) from Formlabs, Somerville, MA, USA	GO was dispersed in acetone, sonicated for 15 min and mixed with resin (0.1, 0.5, and 1 wt% GO); vacuum evaporation of acetone; ultrasonication of resin for 10 min	Formlabs Form 1+ printer, 405 nm, 120 mW power and laser spot size (fwhm) of 155 µm; 50 µm resolution. The printed specimens were cleaned in an isopropyl alcohol (IPA) bath	Annealing in vacuum oven at 50 and 100 °C for 12 h	Electrodes	[111]
GO prepared from graphite powder using a modified Hummers method	A mixture of acrylated monomers and acrylated oligomers (Formlabs, Somerville, MA, USA, flexible Resin, FLFLGR01	GO was dispersed in chloroform using an ultrasonic bath for 1 h; resin addition; ultrasonic mixing for 2 h; stirring at 95 °C for 18 h to remove the solvent; GO content for printing: 0.1–0.3 wt%	SLA 3D printer (Form 1+, Formlabs Inc., MA, USA); washing with IPA	post-curing using an UV-light source	-	[113]

Table 2. *Cont.*

Filler	Polymer Matrix	Resin Preparation	3D Printing Conditions	Post-Processing Steps	Applications	Ref.
Graphene, GO, graphite nanoplatelets	Photocurable acrylic-based resin was Formlabs Clear FLGPCL4 (Formlabs, Somerville, MA, USA)	Dispersion of the nanofiller (0.1 wt%) in the polymer resin; ultrasonication for 30 min; degasification; ultrasonic bath for 15 min	405 nm	-	Biomedical applications	[115]
GO prepared by a modified Hummers' method	Commercial PIC100 resin (EnvisionTEC Inc., Dearborn, MI)	GO (1, 2, 3 wt.%) was mixed with the resin for 24 h by magnetic bar	3D printing was performed using a self-made projection SLA system; light intensity of 3900 μWcm^{-2}; layer thickness of 30 µm	Pyrolysis with a heating rate of 2 °C/min and, following the profile 25–150 °C/ 1 h–300 °C/ 1 h–400 °C/ 1 h–500 °C/3 h	Semiconductors	[120]
Graphene powder	Polylactic acid–polyurethane (PLA-PUA) oligomer	Triethylene glycol dimethacrylate (37 wt%), PLA-PUA (62 wt.%), Irgacure (1 wt%). Dissolution of the initiator in the diluent, addition of graphene (0.5 wt%), ultrasonication, addition of the oligomer, mechanical stirring, degassing.	405 nm SLA (Photon, ANYCUBIC, China); 20 W UV-light intensity; 0.020 m/h print speed; 47 µm XY resolution; 1.25 µm Z axis accuracy; layer thickness from 0.02 mm to 0.2 mm	- [a]	Bone tissue engineering	[117]

[a] Not specified.

Graphene has the potential to become a key candidate as a filler reinforcer in polymer resins for 4D printing to boost the development of smart materials. Four-dimensional printing has potential applications in many fields due to the unique characteristics of the printed structure to undergo a transformation in shape, properties or functionality in time (4th dimension) when it is exposed to an external stimulus (temperature, electric or magnetic field, humid atmosphere etc.) [121]. This strategy can produce 4D biofabricated constructs for regenerative medicine [122], control systems, soft robotics [123], among others. As an example, Chowdhury et al. reported the 4D printing of shape memory polymers based on tert-butyl acrylate and di(ethylene glycol) diacrylate reinforced with 0.1 wt%, 0.3 wt% and 0.5 wt% graphene nanoparticles [123]. The authors stated that the addition of graphene nanoparticles led to an increase in tensile stress, a reduction in surface roughness and a dramatic increase in the recovery time.

In conclusion, the portfolio of graphene-based resins for SLA offers many perspectives to design new hybrid objects with outstanding properties. Up to date, scientists made great progress in attaining superior printability, tunable properties, controlled architectures and biological function of 3D-printed constructs (Figure 5). Future work could support the development of micro-devices for monitoring and therapy, electroactive scaffolds for neurogenesis and myogenesis, membranes in ocular regenerative medicine, among others.

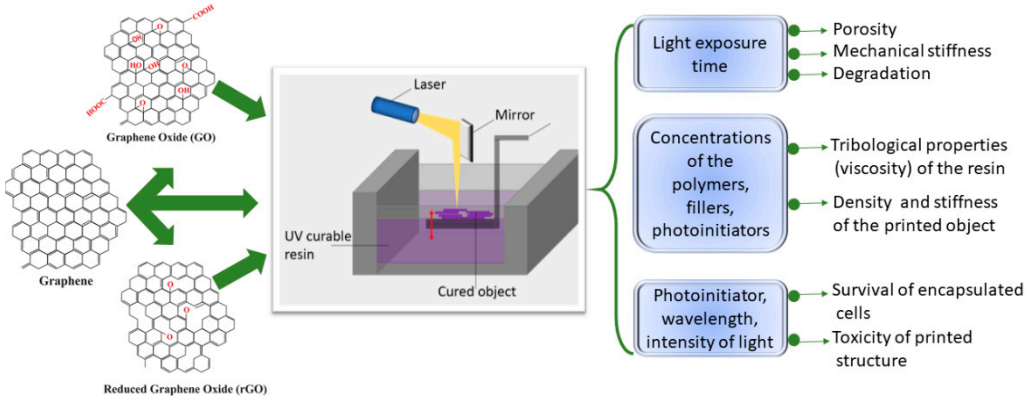


Figure 5. Overview of graphene-based resins for SLA.

4.3. Three-Dimensional SLA Printing of Functionalized Graphene Composites

The interactions between GO and hydrophobic polymer matrix are relatively weak, based on non-covalent interactions, such as hydrogen bonds or van der Waals forces [124]. Consequently, the mechanical toughness of graphene nanocomposites, required for some applications, is lower than expected. The unique opportunities offered by graphene are fully exploited after the functionalization of GO with molecules that enable creation of strong covalent interactions with the surrounding polymer matrix. Some authors reported the functionalization of graphene with photosensitive groups, such as azobenzene [125], and their findings can be implemented in the design of new photocurable resins for SLA. The chemical functionalization of graphene with photoactive units led to the formation of the so-called "photoactive graphene", which undergo a chemical or physical reaction upon exposure to sunlight and/or ultraviolet light [126]. Therefore, their applications are predominantly in the fields of optoelectronics and photocatalysis. Interested readers are referred to other review papers to know more details about the functionalization of graphene and GO [127], as this article pays particular attention to the design of new resins for graphene-based polymer composites. The analysis of selected peer-reviewed literature revealed that the incorporation of unmodified GO into a resin for SLA printing is prevalent. A promising approach refers to the surface modification of graphene, which is helpful for the formation of covalent bonds between nanofiller and polymer matrix, which further determine the effective improvement of mechanical properties. Table 3 summarizes the studies with the most representative results.

Li et al. [128] synthesized 2-hydroxyethyl methacrylate-grafted graphene oxide (HEMA-g-GO) and dispersed it in an acrylate photosensitive resin to prepare nanocomposites via SLA. The results showed that improvements in mechanical strength were obtained by adding small amounts of HEMA-g-GO (0.01, 0.003 and 0.06 wt%). The tensile strength and flexural strength of nanocomposites were increased by 67% and 32%, respectively, for the nanocomposite with 0.06 wt% HEMA-g-GO.

Later, Palaganas et al. [129] has successfully grafted acrylate groups on GO, resulting in improved thermal stability of the filler. The functionalized GO (fGO) was homogeneously dispersed into commercial methacrylate resin and generated good interfacial adhesion that causes effective load transmission from the matrix to the filler in the 3D-printed structure. This material exhibited excellent tensile strength, ductility, and fracture energy with a minor loading of 0.2 wt% GO.

Very recently, de León et al. demonstrated that surface modification reactions of GO with chitosan and alkaline phosphatase could be made after manufacturing the 3D-printed objects [130]. The authors stated that introducing GO in concentration below 1 wt% results in nanocomposites with higher strength and toughness when compared to the pristine resin. The obtained nanocomposites were considered suitable as platforms for the selective immobilization of functional biomolecules.

Table 3. The most representative 3D-printed functionalized graphene-based composites.

Functionalization Agent	Polymer Matrix	Resin Preparation	3D Printing Conditions	Post-Processing Steps	Applications	Ref.
2-Hydroxyethyl methacrylate	Acrylate photosensitive resin synthesized by free radical polymerization	Bisphenol-A epoxy diacrylate (E-44) and diethylene glycol (mole ratio of 10:1) was mixed with butylated hydroxytoluene (0.1 wt%) at 70 °C for 1 h. Tetrabutylammonium bromide and acrylic acid were added, and the mixture was heated at 95 °C for 1 h. Cationic aliphatic epoxy resin, diluent monomer, sensitizer and Irgacure 250 were added. The filler was dispersed by ultrasonication for 1 h.	SLA printer (Hygieo WIZART DLP/SLA, China); UV-light irradiation	-	Different graphene reinforced resins for SLA	[128]

Table 3. *Cont.*

Functionalization Agent	Polymer Matrix	Resin Preparation	3D Printing Conditions	Post-Processing Steps	Applications	Ref.
Acryloyl chloride	Methacrylate-based resin for SLA (Formlabs Somerville, MA, USA)	Filler concentrations: 0−1.0 wt%; ultrasonication for 30 min; continuous stirring at 50 °C for 12 h	25 µm resolution, 405 nm laser wavelength, and 250 mW power rating	2 isopropanol baths for 10 min; drying at RT for 30 min; post-curing at 405 nm at 60 °C for 1 h	Industrial applications, such as drone parts or medical devices	[129]
3-(methacryloyloxy) propyl trimethoxysilane (MEMO)	Epoxy acrylate (BisGMA/1,6 hexane diol diacrylate)	GO synthesised by the Tour method was mixed with MEMO and ethanol for 8 h at room temperature and 2 h at 60 °C. Resin: mixture of bisphenol A glycerolate diacrylate (50%) and hexanediol diacrylate (50%); GO (0.05 ÷ 0.25%), Irgacure 819	SLA printer manufactured at Marmara University Manufacturing Laboratory, 405 nm; 0.1 mm thickness for each layer	Raycon UV System Mercury Lamb Conveyor (speed was 5 min/mm at 150 kV) with a short wavelength (200 nm)	-	[131]
BYK dispersant (copolymer containing amino groups)	Polyester acrylate, acryloylmorpholine (ACMO) as diluent monomer; TPO as photosensitizer	A mixture of graphite oxide, BYK and ethanol was first subjected to a sonochemical exfoliation process for 1 h; centrifugation; washing with ethanol; drying under vacuum at 80 °C. The functionalized GO was mixed with ACMO; ultrasonication for 30 min; addition of TPO and polyester acrylate; magnetic stirring for 1 h. Filler concentrations: 2, 5 and 7 wt%	SLA printer (Xiaofang, China); 25 µm layer thickness; 405 nm wavelength; energy dose of the UV laser of 1327 mJ/cm^2	Annealing at different temperatures (200, 250, 300, and 350 °C) in nitrogen atmosphere for 1 h.	Smart electronics	[132]

5. Problems and Limitations

The 3D printable graphene resins described in previous sections comprise three major components: (1) host polymer, (2) solvent or diluent and (3) graphene/GO in the form of powder or nanoplates. The starting resins are usually of low viscosity (0.25–10 Pa·s) [133]. Commercial resins provided by Formlabs and Covestro uses viscosities between 0.3 and 1.6 Pa·s. In general, is recommended a viscosity lower than 2 Pa·s for SLA 3D printers [134] in order to allow recoating of the resin during SLA 3D printing [135]. Controlling and tuning rheological features is essential to enable 3D printing and requires the incorporation of additional materials, including polymers (polylactic acid, polybutylene terephthalate, lignin) or fumed silica. Binders are also added to provide mechanical integrity to the built objects.

3D printing of graphene-based materials is facing several problems and limitations that still hamper the manufacturing at industrial levels of a large variety of medical or electrical devices, thin films and elastic structures. More specifically, the primary requirement refers to the stability and homogeneity of the dispersions without graphene agglomerates. Secondly, matching the polarity between the polymer and filler makes the interaction between graphene and the polymer matrix stronger [136], which results in superior properties. As for the bioinks, the main drawback is represented by the incorporation of cells into printing materials and their survival after the fabrication process [137]. Ultimately, the cost-effectiveness of the 3D-printed objects.

The 3D-printed structures should reproduce the natural tissue at all levels, i.e., physical and biological, with similar morphological and mechanical characteristics, capable of promoting cells attachment, growth and differentiation. As a result, building biomimetic scaffolds for tissue engineering is not an easy task, and one of the issues relates to porosity and degradability. An interconnected porosity will provide the optimal environment to promote tissue ingrowth but will affect the mechanical strength of the scaffold. AM techniques face some limitations in achieving high porosity in the fabrication of complex 3D scaffolds for tissue engineering. Particularly in SLA, the porosity of the building blocks is usually smaller than the original design due to overcuring in both depth and width [138].

Probably the most important limitation of the conventional stereolithography process is the adherence of the polymerized layers to the solid constraining interface. Some mitigation actions to prevent these stiction forces have been explored, including the use of

a static, inert immiscible liquid below the resin as the constraining interface [139], the use of an oxygen-permeable membrane that inhibits the polymerization of a thin resin layer [140] or by using dual-wavelength irradiation to photopolymerize and simultaneously inhibits the reaction of (meth)acrylate resin at the solid interface [141]. Additionally, the possibility of automatically exchanging the resin reservoirs and the restriction of using one resin at a time is still a technological limitation of the SLA technique.

The functionality of 3D-printed constructs is highly material-dependent [142]. The presence of an additive, especially in a concentration higher than 10%, may hinder the photopolymerization of the resin, and, consequently, the construct presents irregularities and deformities in some parts [143]. Obviously, the presence of graphene results in deep black resins, affecting the penetration of light into the resin and its photocrosslinking behaviour. Graphene oxide has been found to participate in chain termination, and if aggregation occurs, it results in a decrease in their photochemical activity [144]. For now, the use of photocurable materials prevents the scalable development of SLA. Finally, phase separation may occur during the storage of the printable resin.

The ability of the SLA technique to create complex shape prototypes in a rapid manner is overshadowed by the inferior accuracy, brittleness and poor mechanical properties that sometimes are reported for the 3D-printed structures. As is well known, the mechanical properties of the printed objects are directly correlated with their molecular-level structuring, such as crosslink density. A significant challenge is to adapt the speed of printing with the crosslinking rate of the resins developed for SLA. By changing the light intensity and exposure time, the production rate and the number of free radicals can be controlled [145]. Fast curing is necessary to obtain a good resolution, but the reaction grows inhomogeneous, and some produced parts are not fully crosslinked. In general, the fast curable resins do not exhibit cell biocompatibility, and this limits their use in medical applications. All these challenges represent an open-innovation platform to develop new resin formulations.

6. Post-Treatments

During the SLA process, the laser beam is directed preferentially on the outline of each layer to reduce the curing time [62]. Thereby, some amounts of unreactive groups are left inside the built object, affecting its stability and strength. Further post-curing is often used to reinforce the bonding and, thus, improve the quality of the final 3D product [61]. Both UV lamps and ovens are used in post-treatment techniques, but in SLA, the hardening of the uncured resin is prevalently performed by means of a light source. Post-curing is necessary in both SLA configurations (see Section 3) and irrespective of the formulation of photocurable resin in order to achieve higher surface finishes of around 50 microns [146]. Post-processing usually refers to several steps: (1) removal of supports, (2) soaking the printed specimens in ethanol or isopropyl alcohol in order to remove uncured resin and a photoinitiator, and (3) curing [11]. Post-curing process integrating UV and heat guarantees the conversion of the unreacted groups and enhance the mechanical properties of the 3D-printed parts [147].

Acrylate and methacrylate-based resins require post-curing but are prone to shrinkage and warping. Annealing conditions must be selected according to the chemistry of the resin and adapted to the intended application of the 3D-printed product. The strengthening effect of crosslinking is observed at temperatures higher enough to allow chemical reactions between GO and polymer matrix, such as esterification, which are endothermic in nature, but lower enough to prevent polymer degradation and GO reduction [111]. Instead, high-temperature conditions reduce GO to graphene, leading to improved electrical properties of the as-printed architectures [120].

7. Biocompatibility Issues

Any implantable device within the human body must meet regulatory standards for biocompatibility and prove to be nontoxic. The Food and Drug Administration (FDA) is among the regulators that approve any medical device before reaching the market. A

classification of 3D-printed devices includes products with low or no risks, such as bandages and surgical tools and implantable devices [148]. The issues related to their biocompatibility, sterility, cleaning, reproducibility must be solved in order to obtain approval. Ideally, the selection of the printing formulations should consider water-based and biocompatible raw materials. The presence of organic solvents, mostly toxic, requires supplementary purification steps in order to prevent damage to bioprinted living cells and tissues. SLA is, to some extent, compatible with cell-laden resins, but printing must be performed under sterile conditions [149]. With respect to the polymer matrix, either synthetic or natural polymers may be suitable, and some of them have been featured in Section 4.1.

After a survey of the literature, with a focus on the cytotoxicity tests performed on graphene-based materials, some contradictory results were revealed. Some authors concluded that graphene might have potential cytotoxicity risks at even low concentrations [150]. Conversely, other research works have presented the ability of graphene to stimulate cell proliferation [151]. The results showed that the addition of small concentrations (less than 1 wt%) of graphene improved human adipose-derived stem cells (hADSCs) proliferation to poly(ε-caprolactone) (PCL)/graphene scaffolds [151]. It has been reported that graphene provides the requirements to develop successful scaffolds for nerve restoration. This is due to graphene's strong π bond and large surface, which improve cell bioelectricity between scaffolds and cellular membrane [152]. Moreover, the cells showed good survival after the fabrication of the construct. Other studies reported the effect of graphene or graphene oxide on stem cell differentiation into neurogenic [153], chondrogenic [154], myogenic [155] and osteogenic cells [156].

Regarding the polymers used in SLA, acrylates are cytotoxic and cannot be used as scaffold materials but can be replaced with methacrylates, thiol–ene systems, and other photoreactive monomers. For the preparation of cell-laden scaffolds, it is essential that the resin is water-soluble. Up to date, the range of photopolymerizable biomaterials for tissue engineering and regenerative medicine by SLA is quite limited.

8. Conclusions and Future Perspectives

The use of graphene derivatives to obtain 3D scaffolds can have a major impact in the future by capitalizing on one of the two most important properties of these species–mechanical properties and electrical conductivity. The mechanical properties of graphene will be able to allow the obtaining of polymer matrices with applications that require improved mechanical properties, such as cranial meshes or cartilages. Such composites could successfully replace other precursors for scaffolds with high hardness, for example, the replacement of hydroxyapatite for bone implants. The presence of graphene in a polymer matrix can successfully substitute ceramic precursors. Moreover, the presence of graphene in the composite matrix can add osteoinductive properties with spectacular consequences in the integration of the implant into the bone. Electrical conductivity is useful to obtain nerve ducts that allow, in addition to the properties of the material, to solve mechanical and support needs, adding properties so far hard to imagine by creating complex conductive networks. This property could allow the attachment of various sensors that lead to continuous monitoring of the physiologic processes in the implantation area, as well as a new philosophy in the field of diagnosis. Thus, it will be possible to obtain, in real-time, information about the markers of infection or tumours in the case of operations to remove cancerous tumours, concentrations of cations or other biologically active species and even monitoring of the quantities of pharmaceutically active substances used for various diseases. All the excellent properties regarding the electrical conductivity through graphene could be exploited for obtaining muscle tissue. The 3D printing technique can be used to obtain fibrillar structures with motor and contraction capacity; once this problem is solved, organs can be reproduced in their integrity.

AM, and particularly SLA, consist of a layer-by-layer fabrication method that can include the nanofillers, which make them feasible for manufacturing graphene composites with superior mechanical strength. When compared with other bioprinters, SLA printers

have a better resolution capacity and could be used to print with a good precision complex and customizable buildings for the medical field. It was successfully used to fabricate unique constructs for cartilage reconstruction or neural tissue regeneration and scaffolds embedded with various bioactive molecules or multifunctional nanoparticles. Graphene and its derivatives were often introduced in photocurable resins to enhance their mechanical and biochemical functions. The expansion of graphene-based resins will be more consistently after exceeding practical difficulties such as efficiency, cost, dispersiveness in polymers and solvents, limited printability. The main challenges of SLA 3D printing of graphene-based composites include the limited material availability, biocompatibility and degradability of the materials, accuracy and printing speed, pre- and post-processing steps, multimaterial printing, the requirements for increased resolution. To date, the feasibility of mass production and widespread commercialization are unmet goals. Significant advances in the fields of medicine can be achieved by multidisciplinary teams, including cell biologists, engineers, physicists, and doctors. Further research to explore plant oils for the synthesis of new polymers as liquid resins for SLA will enlarge the available biocompatible materials for biomedical scaffolds. More progress in the development of 3D printers and materials is needed to achieve clinical needs and to reveal the full potential of this technology in medicine.

Author Contributions: Conceptualization, analysis of the information, investigation, and writing of the paper, I.C.; writing of the paper, review and editing, Ş.I.V. and D.B. All authors have read and agreed to the published version of the manuscript.

Funding: This work was supported by a grant from the Romanian Ministry of Research and Innovation, CCDI-UEFISCDI, project number PN-III-CEI-BIM-PBE-2020-0014/12BM/2021, within PNCDI III and by the project UPB-Proof of Concept 2020. D.B. acknowledges Romanian National Authority for Scientific Research and Innovation (UEFISCDI), project 5PTE/2020-BIOTEHKER.

Institutional Review Board Statement: Not applicable.

Informed Consent Statement: Not applicable.

Data Availability Statement: Not applicable.

Acknowledgments: The authors are also thankful to Florin Sasu for Figure 1 illustration.

Conflicts of Interest: The authors declare no conflict of interest.

References

1. Loxley, A. Devices and Implants Prepared Using Hot Melt Extrusion. In *Melt Extrusion*; Repka, M., Langley, N., DiNunzio, J., Eds.; AAPS Advances in the Pharmaceutical Sciences Series; Springer: New York, NY, USA, 2013; Volume 9, pp. 281–298. [CrossRef]
2. Jain, S.; Fuoco, T.; Yassin, M.A.; Mustafa, K.; Finne-Wistrand, A. Printability and Critical Insight into Polymer Properties during Direct-Extrusion Based 3D Printing of Medical Grade Polylactide and Copolyesters. *Biomacromolecules* **2020**, *21*, 388–396. [CrossRef] [PubMed]
3. Thavornyutikarn, B.; Chantarapanich, N.; Sitthiseripratip, K.; Thouas, G.A.; Chen, Q. Bone Tissue Engineering Scaffolding: Computer-Aided Scaffolding Techniques. *Prog. Biomater.* **2014**, *3*, 61–102. [CrossRef] [PubMed]
4. Ng, W.L.; Lee, J.M.; Zhou, M.; Chen, Y.-W.; Lee, K.-X.A.; Yeong, W.Y.; Shen, Y.-F. Vat polymerization-based bioprinting—Process, materials, applications and regulatory challenges. *Biofabrication* **2020**, *12*, 022001. [CrossRef]
5. Park, S.-M.; Park, J.-M.; Kim, S.-K.; Heo, S.-J.; Koak, J.-Y. Flexural Strength of 3D-Printing Resin Materials for Provisional Fixed Dental Prostheses. *Materials* **2020**, *13*, 3970. [CrossRef] [PubMed]
6. Alharbi, N.; Osman, R.B.; Wismeijer, D. Factors Influencing the Dimensional Accuracy of 3D-Printed Full-Coverage Dental Restorations Using Stereolithography Technology. *Int. J. Prosthodont.* **2016**, *29*, 503–510. [CrossRef]
7. Pere, C.P.P.; Economidou, S.N.; Lall, G.; Ziraud, C.; Boateng, J.S.; Alexander, B.D.; Lamprou, D.; Douroumis, D. 3D printed microneedles for insulin skin delivery. *Int. J. Pharm.* **2018**, *544*, 425–432. [CrossRef]
8. Wang, Y.; Sun, L.; Mei, Z.; Zhang, F.; He, M.; Fletcher, C.; Wang, F.; Yang, J.; Bi, D.; Jiang, Y.; et al. 3D printed biodegradable implants as an individualized drug delivery system for local chemo-therapy of osteosarcoma. *Mater. Des.* **2020**, *186*, 108336. [CrossRef]
9. Guillaume, O.; Geven, M.; Sprecher, C.; Stadelmann, V.A.; Grijpma, D.W.; Tang, T.T.; Qin, L.; Lai, Y.; Alini, M.; De Bruijn, J.; et al. Surface-enrichment with hydroxyapatite nanoparticles in stereolithography-fabricated composite polymer scaffolds promotes bone repair. *Acta Biomater.* **2017**, *54*, 386–398. [CrossRef]

10. Heidt, B.; Rogosic, R.; Bonni, S.; Passariello-Jansen, J.; Dimech, D.; Lowdon, J.W.; Arreguin-Campos, R.; Redeker, E.S.; Eersels, K.; Diliën, H.; et al. The Liberalization of Microfluidics: Form 2 Benchtop 3D Printing as an Affordable Alternative to Established Manufacturing Methods. *Phys. Status Solidi* **2020**, *217*, 1900935. [CrossRef]
11. Pagac, M.; Hajnys, J.; Ma, Q.-P.; Jancar, L.; Jansa, J.; Stefek, P.; Mesicek, J. A Review of Vat Photopolymerization Technology: Materials, Applications, Challenges, and Future Trends of 3D Printing. *Polymers* **2021**, *13*, 598. [CrossRef]
12. Xu, X.; Awad, A.; Robles-Martinez, P.; Gaisford, S.; Goyanes, A.; Basit, A.W. Vat photopolymerization 3D printing for advanced drug delivery and medical device applications. *J. Control. Release* **2020**, *329*, 743–757. [CrossRef] [PubMed]
13. Schubert, U.S.; Wloka, T.; Gottschaldt, M. From light to structure: Photo initiators in two-photon polymerization. *Chem. A Eur. J.* **2022**. [CrossRef] [PubMed]
14. Nguyen, A.K.; Narayan, R.J. Two-photon polymerization for biological applications. *Mater. Today* **2017**, *20*, 314–322. [CrossRef]
15. Zheng, Y.; Huang, X.; Chen, J.; Wu, K.; Wang, J.; Zhang, X. A Review of Conductive Carbon Materials for 3D Printing: Materials, Technologies, Properties, and Applications. *Materials* **2021**, *14*, 3911. [CrossRef] [PubMed]
16. Huang, C.-T.; Shrestha, L.K.; Ariga, K.; Hsu, S.-H. A graphene–polyurethane composite hydrogel as a potential bioink for 3D bioprinting and differentiation of neural stem cells. *J. Mater. Chem. B* **2017**, *5*, 8854–8864. [CrossRef]
17. Voicu, S.I.; Pandele, M.A.; Vasile, E.; Rughinis, R.; Crica, L.; Pilan, L.; Ionita, M. The impact of sonication time through polysulfone-graphene oxide composite films properties. *Dig. J. Nanomater. Biostruct.* **2013**, *8*, 1389–1394.
18. Ionita, M.; Vasile, E.; Crica, L.E.; Voicu, S.I.; Pandele, A.M.; Dinescu, S.; Predoiu, L.; Galateanu, B.; Hermenean, A.; Costache, M. Synthesis, characterization and in vitro studies of polysulfone/graphene oxide composite membranes. *Compos. Part B Eng.* **2015**, *72*, 108–115. [CrossRef]
19. Ionita, M.; Crica, L.E.; Voicu, S.I.; Pandele, A.M.; Iovu, H. Fabrication of cellulose triacetate/graphene oxide porous membrane. *Polym. Adv. Technol.* **2015**, *27*, 350–357. [CrossRef]
20. Ioniță, M.; Crică, L.E.; Voicu, S.I.; Dinescu, S.; Miculescu, F.; Costache, M.; Iovu, H. Synergistic effect of carbon nanotubes and graphene for high performance cellulose acetate membranes in biomedical applications. *Carbohydr. Polym.* **2018**, *183*, 50–61. [CrossRef]
21. Palla-Papavlu, A.; Voicu, S.; Dinescu, M. Sensitive Materials and Coating Technologies for Surface Acoustic Wave Sensors. *Chemosensors* **2021**, *9*, 105. [CrossRef]
22. Bonciu, A.F.; Filipescu, M.; Voicu, S.I.; Lippert, T.; Palla-Papavlu, A. Facile Fabrication of Hybrid Carbon Nanotube Sensors by Laser Direct Transfer. *Nanomaterials* **2021**, *11*, 2604. [CrossRef]
23. Muhulet, A.; Miculescu, F.; Voicu, S.I.; Schütt, F.; Thakur, V.K.; Mishra, Y.K.; Costache, M.; Iovu, H. Fundamentals and scopes of doped carbon nanotubes towards energy and biosensing applications. *Mater. Today Energy* **2018**, *9*, 154–186. [CrossRef]
24. Ioniţă, M.; Vlăsceanu, G.M.; Watzlawek, A.A.; Voicu, S.I.; Burns, J.S.; Iovu, H. Graphene and functionalized graphene: Extraordinary prospects for nanobiocomposite materials. *Compos. Part B Eng.* **2017**, *121*, 34–57. [CrossRef]
25. Muhulet, A.; Tuncel, C.; Miculescu, F.; Pandele, A.M.; Bobirica, C.; Orbeci, C.; Bobirica, L.; Palla-Papavlu, A.; Voicu, S.I. Synthesis and characterization of polysulfone–TiO_2 decorated MWCNT composite membranes by sonochemical method. *Appl. Phys. A* **2020**, *126*, 233. [CrossRef]
26. Pandele, A.M.; Serbanescu, O.S.; Voicu, S.I. Polysulfone Composite Membranes with Carbonaceous Structure: Synthesis and Applications. *Coatings* **2020**, *10*, 609. [CrossRef]
27. Oprea, M.; Voicu, S.I. Recent Advances in Applications of Cellulose Derivatives-Based Composite Membranes with Hydroxyapatite. *Materials* **2020**, *13*, 2481. [CrossRef]
28. Oprea, M.; Voicu, S.I. Cellulose Composites with Graphene for Tissue Engineering Applications. *Materials* **2020**, *13*, 5347. [CrossRef]
29. Pandele, A.M.; Iovu, H.; Orbeci, C.; Tuncel, C.; Miculescu, F.; Nicolescu, A.; Deleanu, C.; Voicu, S.I. Surface modified cellulose acetate membranes for the reactive retention of tetracycline. *Sep. Purif. Technol.* **2020**, *249*, 117145. [CrossRef]
30. Serbanescu, O.S.; Voicu, S.I.; Thakur, V.K. Polysulfone functionalized membranes: Properties and challenges. *Mater. Today Chem.* **2020**, *17*, 100302. [CrossRef]
31. Pandele, A.M.; Oprea, M.; Dutu, A.A.; Miculescu, F.; Voicu, S.I. A Novel Generation of Polysulfone/Crown Ether-Functionalized Reduced Graphene Oxide Membranes with Potential Applications in Hemodialysis. *Polymers* **2021**, *14*, 148. [CrossRef]
32. Mohan, V.B.; Lau, K.-T.; Hui, D.; Bhattacharyya, D. Graphene-based materials and their composites: A review on production, applications and product limitations. *Compos. Part B Eng.* **2018**, *142*, 200–220. [CrossRef]
33. Ponnamma, D.; Yin, Y.; Salim, N.; Parameswaranpillai, J.; Thomas, S.; Hameed, N. Recent progress and multifunctional applications of 3D printed graphene nanocomposites. *Compos. Part B Eng.* **2020**, *204*, 108493. [CrossRef]
34. Catania, F.; Marras, E.; Giorcelli, M.; Jagdale, P.; Lavagna, L.; Tagliaferro, A.; Bartoli, M. A Review on Recent Advancements of Graphene and Graphene-Related Materials in Biological Applications. *Appl. Sci.* **2021**, *11*, 614. [CrossRef]
35. Vlăsceanu, G.M.; Iovu, H.; Ioniţă, M. Graphene inks for the 3D printing of cell culture scaffolds and related molecular arrays. *Compos. Part B Eng.* **2019**, *162*, 712–723. [CrossRef]
36. Li, Y.; Feng, Z.; Huang, L.; Essa, K.; Bilotti, E.; Zhang, H.; Peijs, T.; Hao, L. Additive manufacturing high performance graphene-based composites: A review. *Compos. Part A Appl. Sci. Manuf.* **2019**, *124*. [CrossRef]
37. Pal, N.; Banerjee, S.; Roy, P.; Pal, K. Melt-blending of unmodified and modified cellulose nanocrystals with reduced graphene oxide into PLA matrix for biomedical application. *Polym. Adv. Technol.* **2019**, *30*, 3049–3060. [CrossRef]

38. Grant, J.J.; Pillai, S.C.; Hehir, S.; McAfee, M.; Breen, A. Biomedical Applications of Electrospun Graphene Oxide. *ACS Biomater. Sci. Eng.* **2021**, *7*, 1278–1301. [CrossRef] [PubMed]
39. Bahrami, S.; Solouk, A.; Mirzadeh, H.; Seifalian, A.M. Electroconductive polyurethane/graphene nanocomposite for biomedical applications. *Compos. Part B Eng.* **2019**, *168*, 421–431. [CrossRef]
40. Nekounam, H.; Gholizadeh, S.; Allahyari, Z.; Samadian, H.; Nazeri, N.; Shokrgozar, M.A.; Faridi-Majidi, R. Electroconductive scaffolds for tissue regeneration: Current opportunities, pitfalls, and potential solutions. *Mater. Res. Bull.* **2020**, *134*, 111083. [CrossRef]
41. Khan, Y.H.; Islam, A.; Sarwar, A.; Gull, N.; Khan, S.M.; Munawar, A.; Zia, S.; Sabir, A.; Shafiq, M.; Jamil, T. Novel green nano composites films fabricated by indigenously synthesized graphene oxide and chitosan. *Carbohydr. Polym.* **2016**, *146*, 131–138. [CrossRef]
42. Yang, J.-H.; Lin, S.-H.; Lee, Y.-D. Preparation and characterization of poly(l-lactide)–graphene composites using the in situ ring-opening polymerization of PLLA with graphene as the initiator. *J. Mater. Chem.* **2012**, *22*, 10805–10815. [CrossRef]
43. Zhang, J.; Zhang, C.; Madbouly, S.A. In situ polymerization of bio-based thermosetting polyurethane/graphene oxide nanocomposites. *J. Appl. Polym. Sci.* **2015**, *132*, 41751. [CrossRef]
44. Shin, S.R.; Bolagh, B.A.G.; Gao, X.; Nikkhah, M.; Jung, S.M.; Dolatshahi-Pirouz, A.; Kim, S.B.; Kim, S.M.; Dokmeci, M.R.; Tang, X.; et al. Layer-by-Layer Assembly of 3D Tissue Constructs with Functionalized Graphene. *Adv. Funct. Mater.* **2014**, *24*, 6136–6144. [CrossRef]
45. Chaitoglou, S.; Spachis, L.; Zisis, G.; Raptis, I.; Papanikolaou, N.; Vavouliotis, A.; Penedo, R.; Fernandes, N.; Dimoulas, A. Layer-by-layer assembled graphene coatings on polyurethane films as He permeation barrier. *Prog. Org. Coatings* **2020**, *150*, 105984. [CrossRef]
46. Khan, M.U.A.; Haider, S.; Haider, A.; Razak, S.I.A.; Kadir, M.R.A.; Shah, S.A.; Javed, A.; Shakir, I.; Al-Zahrani, A.A. Development of porous, antibacterial and biocompatible GO/n-HAp/bacterial cellulose/β-glucan biocomposite scaffold for bone tissue engineering. *Arab. J. Chem.* **2021**, *14*, 102924. [CrossRef]
47. Verma, D.; Goh, K.L. Chapter 11—Functionalized Graphene-Based Nanocomposites for Energy Applications. In *Functionalized Graphene Nanocomposites and Their Derivatives*; Jawaid, M., Bouhfid, R., Qaiss, A.E.K., Eds.; Elsevier: Amsterdam, The Netherlands, 2019; pp. 219–243. [CrossRef]
48. Ivanoska-Dacikj, A.; Bogoeva-Gaceva, G. Chapter Two—Fabrication Methods of Carbon-Based Rubber Nanocomposites. In *Carbon-Based Nanofillers and Their Rubber Nanocomposites*; Yaragalla, S., Ed.; Elsevier: Amsterdam, The Netherlands, 2019; pp. 27–47. [CrossRef]
49. Platnieks, O.; Gaidukovs, S.; Neibolts, N.; Barkane, A.; Gaidukova, G.; Thakur, V. Poly(butylene succinate) and graphene nanoplatelet–based sustainable functional nanocomposite materials: Structure-properties relationship. *Mater. Today Chem.* **2020**, *18*, 100351. [CrossRef]
50. Popescu, M.-T.; Tasis, D.; Papadimitriou, K.D.; Gkermpoura, S.; Galiotis, C.; Tsitsilianis, C. Colloidal stabilization of graphene sheets by ionizable amphiphilic block copolymers in various media. *RSC Adv.* **2015**, *5*, 89447–89460. [CrossRef]
51. Paydayesh, A.; Mousavi, S.R.; Estaji, S.; Khonakdar, H.A.; Nozarinya, M.A. Functionalized graphene nanoplatelets/poly (lactic acid)/chitosan nanocomposites: Mechanical, biodegradability, and electrical conductivity properties. *Polym. Compos.* **2022**, *43*, 411–421. [CrossRef]
52. Zhang, C.; Tjiu, W.W.; Fan, W.; Huang, S.; Liu, T. A novel approach for transferring water-dispersible graphene nanosheets into organic media. *J. Mater. Chem.* **2012**, *22*, 11748–11754. [CrossRef]
53. Barroso-Bujans, F.; Cerveny, S.; Verdejo, R.; del Val, J.; Alberdi, J.; Alegria, A.; Colmenero, J. Permanent adsorption of organic solvents in graphite oxide and its effect on the thermal exfoliation. *Carbon* **2010**, *48*, 1079–1087. [CrossRef]
54. Robinson, A.J.; Pérez-Nava, A.; Ali, S.C.; González-Campos, J.B.; Holloway, J.L.; Cosgriff-Hernandez, E.M. Comparative analysis of fiber alignment methods in electrospinning. *Matter* **2021**, *4*, 821–844. [CrossRef]
55. Shi, X.; Zhou, W.; Ma, D.; Ma, Q.; Bridges, D.; Ma, Y.; Hu, A. Electrospinning of Nanofibers and Their Applications for Energy Devices. *J. Nanomater.* **2015**, *2015*, 1–20. [CrossRef]
56. Mao, H.-N.; Wang, X.-G. Use of in-situ polymerization in the preparation of graphene/polymer nanocomposites. *New Carbon Mater.* **2020**, *35*, 336–343. [CrossRef]
57. Dalai, N.; Sreekanth, P.S.R. Mechanical properties of graphene and nano-diamond reinforced ultra high molecular weight polyethylene. *Mater. Today Proc.* **2020**, *27*, 1013–1016. [CrossRef]
58. Melchels, F.P.W.; Feijen, J.; Grijpma, D.W. A review on stereolithography and its applications in biomedical engineering. *Biomaterials* **2010**, *31*, 6121–6130. [CrossRef] [PubMed]
59. Zakeri, S.; Vippola, M.; Levänen, E. A comprehensive review of the photopolymerization of ceramic resins used in stereolithography. *Addit. Manuf.* **2020**, *35*, 101177. [CrossRef]
60. Voet, V.S.D.; Guit, J.; Loos, K. Sustainable Photopolymers in 3D Printing: A Review on Biobased, Biodegradable, and Recyclable Alternatives. *Macromol. Rapid Commun.* **2020**, *42*, e20004752020. [CrossRef]
61. Ashish, M.; Nabeel, A.; Gopinath, P.; Vinogradov, A. Chapter 1—3D Printing in Medicine: Current Challenges and Potential Applications. In *3D Printing Technology in Nanomedicine*; Ahmad, N., Gopinath, P., Dutta, R., Eds.; Elsevier: Amsterdam, The Netherlands, 2019; pp. 1–22. [CrossRef]

62. Taormina, G.; Sciancalepore, C.; Messori, M.; Bondioli, F. 3D printing processes for photocurable polymeric materials: Technologies, materials, and future trends. *J. Appl. Biomater. Funct. Mater.* **2018**, *16*, 151–160. [CrossRef]
63. Bhushan, B.; Caspers, M. An overview of additive manufacturing (3D printing) for microfabrication. *Microsyst. Technol.* **2017**, *23*, 1117–1124. [CrossRef]
64. Schlotthauer, T.; Nolan, D.; Middendorf, P. Influence of short carbon and glass fibers on the curing behavior and accuracy of photopolymers used in stereolithography. *Addit. Manuf.* **2021**, *42*, 102005. [CrossRef]
65. Chiulan, I.; Heggset, E.B.; Voicu, S.I.; Chinga-Carrasco, G. Photopolymerization of Bio-Based Polymers in a Biomedical Engineering Perspective. *Biomacromolecules* **2021**, *22*, 1795–1814. [CrossRef] [PubMed]
66. Bagheri, A.; Jin, J. Photopolymerization in 3D Printing. *ACS Appl. Polym. Mater.* **2019**, *1*, 593–611. [CrossRef]
67. Farzan, A.; Borandeh, S.; Ezazi, N.Z.; Lipponen, S.; Santos, H.A.; Seppälä, J. 3D scaffolding of fast photocurable polyurethane for soft tissue engineering by stereolithography: Influence of materials and geometry on growth of fibroblast cells. *Eur. Polym. J.* **2020**, *139*, 109988. [CrossRef]
68. Zhou, X.; Nowicki, M.; Cui, H.; Zhu, W.; Fang, X.; Miao, S.; Lee, S.-J.; Keidar, M.; Zhang, L.G. 3D bioprinted graphene oxide-incorporated matrix for promoting chondrogenic differentiation of human bone marrow mesenchymal stem cells. *Carbon N. Y.* **2017**, *116*, 615–624. [CrossRef]
69. Elomaa, L.; Keshi, E.; Sauer, I.M.; Weinhart, M. Development of GelMA/PCL and dECM/PCL resins for 3D printing of acellular in vitro tissue scaffolds by stereolithography. *Mater. Sci. Eng. C* **2020**, *112*, 110958. [CrossRef] [PubMed]
70. Miao, S.; Zhu, W.; Castro, N.; Nowicki, M.; Zhou, X.; Cui, H.; Fisher, J.P.; Zhang, L.G. 4D printing smart biomedical scaffolds with novel soybean oil epoxidized acrylate. *Sci. Rep.* **2016**, *6*, 27226. [CrossRef]
71. Guit, J.; Tavares, M.B.L.; Hul, J.; Ye, C.; Loos, K.; Jager, J.; Folkersma, R.; Voet, V.S.D. Photopolymer Resins with Biobased Methacrylates Based on Soybean Oil for Stereolithography. *ACS Appl. Polym. Mater.* **2020**, *2*, 949–957. [CrossRef]
72. Skliutas, E.; Lebedevaite, M.; Kasetaite, S.; Rekštytė, S.; Lileikis, S.; Ostrauskaite, J.; Malinauskas, M. A Bio-Based Resin for a Multi-Scale Optical 3D Printing. *Sci. Rep.* **2020**, *10*, 9758. [CrossRef]
73. Barkane, A.; Platnieks, O.; Jurinovs, M.; Kasetaite, S.; Ostrauskaite, J.; Gaidukovs, S.; Habibi, Y. UV-Light Curing of 3D Printing Inks from Vegetable Oils for Stereolithography. *Polymers* **2021**, *13*, 1195. [CrossRef]
74. Branciforti, D.S.; Lazzaroni, S.; Milanese, C.; Castiglioni, M.; Auricchio, F.; Pasini, D.; Dondi, D. Visible light 3D printing with epoxidized vegetable oils. *Addit. Manuf.* **2018**, *25*, 317–324. [CrossRef]
75. Liang, B.; Li, R.; Zhang, C.; Yang, Z.; Yuan, T. Synthesis and characterization of a novel tri-functional bio-based methacrylate prepolymer from castor oil and its application in UV-curable coatings. *Ind. Crop. Prod.* **2019**, *135*, 170–178. [CrossRef]
76. Hu, Y.; Shang, Q.; Bo, C.; Jia, P.; Feng, G.; Zhang, F.; Liu, C.; Zhou, Y. Synthesis and Properties of UV-Curable Polyfunctional Polyurethane Acrylate Resins from Cardanol. *ACS Omega* **2019**, *4*, 12505–12511. [CrossRef]
77. Grigoryan, B.; Sazer, D.W.; Avila, A.; Albritton, J.L.; Padhye, A.; Ta, A.H.; Greenfield, P.T.; Gibbons, D.L.; Miller, J.S. Development, characterization, and applications of multi-material stereolithography bioprinting. *Sci. Rep.* **2021**, *11*, 3171. [CrossRef] [PubMed]
78. Zhu, W.; Harris, B.T.; Zhang, L.G. Gelatin methacrylamide hydrogel with graphene nanoplatelets for neural cell-laden 3D bioprinting. *Annu. Int. Conf. IEEE Eng. Med. Boil. Soc.* **2016**, *2016*, 4185–4188. [CrossRef]
79. Dash, G.; Pattanaik, S.R.; Behera, S. Graphene for Electron Devices: The Panorama of a Decade. *IEEE J. Electron Devices Soc.* **2014**, *2*, 77–104. [CrossRef]
80. Randviir, E.P.; Brownson, D.A.C.; Banks, C.E. A decade of graphene research: Production, applications and outlook. *Mater. Today* **2014**, *17*, 426–432. [CrossRef]
81. Hummers, W.S.; Offeman, R.E. Preparation of Graphitic Oxide. *J. Am. Chem. Soc.* **1958**, *80*, 1339. [CrossRef]
82. Le, G.T.; Manyam, J.; Opaprakasit, P.; Chanlek, N.; Grisdanurak, N.; Sreearunothai, P. Divergent mechanisms for thermal reduction of graphene oxide and their highly different ion affinities. *Diam. Relat. Mater.* **2018**, *89*, 246–256. [CrossRef]
83. Gómez-Navarro, C.; Weitz, R.T.; Bittner, A.M.; Scolari, M.; Mews, A.; Burghard, M.; Kern, K. Electronic Transport Properties of Individual Chemically Reduced Graphene Oxide Sheets. *Nano Lett.* **2007**, *7*, 3499–3503. [CrossRef]
84. Tung, V.; Allen, M.J.; Yang, Y.; Kaner, R.B. High-throughput solution processing of large-scale graphene. *Nat. Nanotechnol.* **2008**, *4*, 25–29. [CrossRef] [PubMed]
85. De Silva, K.K.H.; Huang, H.-H.; Joshi, R.K.; Yoshimura, M. Chemical reduction of graphene oxide using green reductants. *Carbon* **2017**, *119*, 190–199. [CrossRef]
86. Chen, Y.; Zhao, Y.; Han, D.; Fu, D.; Chen, Y.; Zhou, D.; Li, Y.; Wang, X.; Zhao, Z. A graphite enclosure assisted synthesis of high-quality patterned graphene on 6H–SiC by ion implantation. *Carbon* **2021**, *172*, 353–359. [CrossRef]
87. Kim, J.; Kim, H.-Y.; Jeon, J.H.; An, S.; Hong, J.; Kim, J. Study on the formation of graphene by ion implantation on Cu, Ni and CuNi alloy. *Appl. Surf. Sci.* **2018**, *451*, 162–168. [CrossRef]
88. Li, Z.; Young, R.J.; Backes, C.; Zhao, W.; Zhang, X.; Zhukov, A.; Tillotson, E.; Conlan, A.P.; Ding, F.; Haigh, S.J.; et al. Mechanisms of Liquid-Phase Exfoliation for the Production of Graphene. *ACS Nano* **2020**, *14*, 10976–10985. [CrossRef] [PubMed]
89. Amiri, A.; Naraghi, M.; Ahmadi, G.; Soleymaniha, M.; Shanbedi, M. A review on liquid-phase exfoliation for scalable production of pure graphene, wrinkled, crumpled and functionalized graphene and challenges. *FlatChem* **2018**, *8*, 40–71. [CrossRef]
90. Briggs, N.; Gebeyehu, Z.M.; Vera, A.; Zhao, T.; Wang, K.; Duran, A.D.L.F.; Bersch, B.; Bowen, T.; Knappenberger, K.L.; Robinson, J.A. Epitaxial graphene/silicon carbide intercalation: A minireview on graphene modulation and unique 2D materials. *Nanoscale* **2019**, *11*, 15440–15447. [CrossRef] [PubMed]

91. Mishra, N.; Boeckl, J.J.; Tadich, A.; Jones, R.; Pigram, P.; Edmonds, M.; Fuhrer, M.; Nichols, B.M.; Iacopi, F. Solid source growth of graphene with Ni–Cu catalysts: Towards high quality in situ graphene on silicon. *J. Phys. D Appl. Phys.* **2017**, *50*, 095302. [CrossRef]
92. Papon, R.; Pierlot, C.; Sharma, S.; Shinde, S.M.; Kalita, G.; Tanemura, M. Optimization of CVD parameters for graphene synthesis through design of experiments. *Phys. Status Solidi* **2016**, *254*, 1600629. [CrossRef]
93. Moon, J.-Y.; Kim, S.-I.; Son, S.-K.; Kang, S.-G.; Lim, J.-Y.; Lee, D.K.; Ahn, B.; Whang, D.; Yu, H.K.; Lee, J.-H. An Eco-Friendly, CMOS-Compatible Transfer Process for Large-Scale CVD-Graphene. *Adv. Mater. Interfaces* **2019**, *6*, 1900084. [CrossRef]
94. DeArmond, D.; Zhang, L.; Malik, R.; Reddy, K.V.K.; Alvarez, N.T.; Haase, M.R.; Hsieh, Y.-Y.; Kanakaraj, S.N.; Oslin, N.; Brunemann, J.; et al. Scalable CVD synthesis of three-dimensional graphene from cast catalyst. *Mater. Sci. Eng. B* **2020**, *254*, 114510. [CrossRef]
95. Younis, M.R.; He, G.; Lin, J.; Huang, P. Recent Advances on Graphene Quantum Dots for Bioimaging Applications. *Front. Chem.* **2020**, *8*, 424. [CrossRef] [PubMed]
96. Voicu, S.I.; Thakur, V.K. Graphene-based composite membranes for nanofiltration: Performances and future perspectives. *Emergent Mater.* **2021**, 1–13. [CrossRef]
97. Ferrari, A.C.; Bonaccorso, F.; Fal'Ko, V.; Novoselov, K.S.; Roche, S.; Bøggild, P.; Borini, S.; Koppens, F.H.L.; Palermo, V.; Pugno, N.; et al. Science and technology roadmap for graphene, related two-dimensional crystals, and hybrid systems. *Nanoscale* **2015**, *7*, 4598–4810. [CrossRef] [PubMed]
98. Parizi, M.T.; Ebrahimi, G.; Ezatpour, H. Effect of graphene nanoplatelets content on the micro-structural and mechanical properties of AZ80 magnesium alloy. *Mater. Sci. Eng. A* **2019**, *742*, 373–389. [CrossRef]
99. Chen, Y.; Xu, P.; Shu, Z.; Wu, M.; Wang, L.; Zhang, S.; Zheng, Y.; Chen, H.; Wang, J.; Li, Y.; et al. Multifunctional Graphene Oxide-based Triple Stimuli-Responsive Nanotheranostics. *Adv. Funct. Mater.* **2014**, *24*, 4386–4396. [CrossRef]
100. Thakur, S.; Karak, N. Multi-stimuli responsive smart elastomeric hyperbranched polyurethane/reduced graphene oxide nanocomposites. *J. Mater. Chem. A* **2014**, *2*, 14867–14875. [CrossRef]
101. Salem, M.L.; Gemeay, A.; Gomaa, S.; Aldubayan, M.A.; Assy, L. Superparamagnetic graphene oxide/magnetite nanocomposite delivery system for doxorubicin-induced distinguished tumor cell cycle arrest and apoptosis. *J. Nanopart. Res.* **2020**, *22*, 219. [CrossRef]
102. Gu, Z.; Zhu, S.; Yan, L.; Zhao, F.; Zhao, Y. Graphene-Based Smart Platforms for Combined Cancer Therapy. *Adv. Mater.* **2018**, *31*, e18006622018. [CrossRef]
103. Yang, S.; Lei, P.; Shan, Y.; Zhang, D. Preparation and characterization of antibacterial electrospun chitosan/poly (vinyl alcohol)/graphene oxide composite nanofibrous membrane. *Appl. Surf. Sci.* **2018**, *435*, 832–840. [CrossRef]
104. Liu, Y.; Song, R.; Zhang, X.; Zhang, D. Enhanced antimicrobial activity and pH-responsive sustained release of chitosan/poly (vinyl alcohol)/graphene oxide nanofibrous membrane loading with allicin. *Int. J. Biol. Macromol.* **2020**, *161*, 1405–1413. [CrossRef]
105. Olad, A.; Hagh, H.B.K. Graphene oxide and amin-modified graphene oxide incorporated chitosan-gelatin scaffolds as promising materials for tissue engineering. *Compos. Part B Eng.* **2019**, *162*, 692–702. [CrossRef]
106. Zambrano-Andazol, I.; Vázquez, N.; Chacón, M.; Sánchez-Avila, R.M.; Persinal, M.; Blanco, C.; González, Z.; Menéndez, R.; Sierra, M.; Fernández-Vega, A.; et al. Reduced graphene oxide membranes in ocular regenerative medicine. *Mater. Sci. Eng. C* **2020**, *114*, 111075. [CrossRef] [PubMed]
107. Cheng, Z.; Landish, B.; Chi, Z.; Nannan, C.; Jingyu, D.; Sen, L.; Xiangjin, L. 3D printing hydrogel with graphene oxide is functional in cartilage protection by influencing the signal pathway of Rank/Rankl/OPG. *Mater. Sci. Eng. C* **2017**, *82*, 244–252. [CrossRef] [PubMed]
108. Wei, X.; Li, D.; Jiang, W.; Gu, Z.; Wang, X.; Zhang, Z.; Sun, Z. 3D Printable Graphene Composite. *Sci. Rep.* **2015**, *5*, 11181. [CrossRef] [PubMed]
109. García-Tuñón, E.; Feilden, E.; Zheng, H.; D'Elia, E.; Leong, A.; Saiz, E. Graphene Oxide: An All-in-One Processing Additive for 3D Printing. *ACS Appl. Mater. Interfaces* **2017**, *9*, 32977–32989. [CrossRef] [PubMed]
110. Lin, D.; Jin, S.; Zhang, F.; Wang, C.; Wang, Y.; Zhou, C.; Cheng, G. 3D stereolithography printing of graphene oxide reinforced complex architectures. *Nanotechnology* **2015**, *26*, 434003. [CrossRef]
111. Manapat, J.Z.; Mangadlao, J.D.; Tiu, B.D.B.; Tritchler, G.C.; Advincula, R.C. High-Strength Stereolithographic 3D Printed Nanocomposites: Graphene Oxide Metastability. *ACS Appl. Mater. Interfaces* **2017**, *9*, 10085–10093. [CrossRef]
112. Xiao, R.; Ding, M.; Wang, Y.; Gao, L.; Fan, R.; Lu, Y. Stereolithography (SLA) 3D printing of carbon fiber-graphene oxide (CF-GO) reinforced polymer lattices. *Nanotechnology* **2021**, *32*, 235702. [CrossRef]
113. Tsang, C.H.A.; Zhakeyev, A.; Leung, D.Y.C.; Xuan, J. GO-modified flexible polymer nanocomposites fabricated via 3D stereolithography. *Front. Chem. Sci. Eng.* **2019**, *13*, 736–743. [CrossRef]
114. Lim, S.M.; Shin, B.S.; Kim, K. Characterization of Products Using Additive Manufacturing with Graphene/Photopolymer-Resin Nano-Fluid. *J. Nanosci. Nanotechnol.* **2017**, *17*, 5492–5495. [CrossRef]
115. Lopez de Armentia, S.; Fernández-Villamarín, S.; Ballesteros, Y.; Del Real, J.C.; Dunne, N.; Paz, E. 3D Printing of a Graphene-Modified Photopolymer Using Stereolithography for Biomedical Applications: A Study of the Polymerization Reaction. *Int. J. Bioprinting* **2022**, *8*, 1–16. [CrossRef]
116. Wang, D.; Huang, X.; Li, J.; He, B.; Liu, Q.; Hu, L.; Jiang, G. 3D printing of graphene-doped target for "matrix-free" laser desorption/ionization mass spectrometry. *Chem. Commun.* **2018**, *54*, 2723–2726. [CrossRef] [PubMed]

117. Feng, Z.; Li, Y.; Hao, L.; Yang, Y.; Tang, T.; Tang, D.; Xiong, W. Graphene-Reinforced Biodegradable Resin Composites for Stereolithographic 3D Printing of Bone Structure Scaffolds. *J. Nanomater.* **2019**, *2019*, 9710264. [CrossRef]
118. Mohan, D.; Sajab, M.S.; Kaco, H.; Bakarudin, S.B.; Noor, A.M. 3D Printing of UV-Curable Polyurethane Incorporated with Surface-Grafted Nanocellulose. *Nanomaterials* **2019**, *9*, 1726. [CrossRef] [PubMed]
119. Ibrahim, F.; Mohan, D.; Sajab, M.S.; Bakarudin, S.B.; Kaco, H. Evaluation of the Compatibility of Organosolv Lignin-Graphene Nanoplatelets with Photo-Curable Polyurethane in Stereolithography 3D Printing. *Polymers* **2019**, *11*, 1544. [CrossRef]
120. Korhonen, H.; Sinh, L.H.; Luong, N.D.; Lehtinen, P.; Verho, T.; Partanen, J.; Seppälä, J. Fabrication of graphene-based 3D structures by stereolithography. *Phys. Status Solidi* **2015**, *213*, 982–985. [CrossRef]
121. Ding, A.; Jeon, O.; Cleveland, D.; Gasvoda, K.L.; Wells, D.; Lee, S.J.; Alsberg, E. Jammed Micro-Flake Hydrogel for Four-Dimensional Living Cell Bioprinting. *Adv. Mater.* **2022**, 2109394. [CrossRef]
122. Ding, A.; Lee, S.J.; Ayyagari, S.; Tang, R.; Huynh, C.T.; Alsberg, E. 4D biofabrication via instantly generated graded hydrogel scaffolds. *Bioact. Mater.* **2021**, *7*, 324–332. [CrossRef]
123. Chowdhury, J.; Anirudh, P.V.; Karunakaran, C.; Rajmohan, V.; Mathew, A.T.; Koziol, K.; Alsanie, W.F.; Kannan, C.; Balan, A.S.S.; Thakur, V.K. 4D Printing of Smart Polymer Nanocomposites: Integrating Graphene and Acrylate Based Shape Memory Polymers. *Polymers* **2021**, *13*, 3660. [CrossRef]
124. Mangadlao, J.D.; Huang, R.; Foster, E.L.; Pangilinan, K.D.; Danda, C.; Advincula, A.; Maia, J.M.; Advincula, R.C. Graphene Oxide-Poly(ethylene glycol) methyl ether methacrylate Nanocomposite Hydrogels. *Macromol. Chem. Phys.* **2016**, *217*, 101–107. [CrossRef]
125. Deepshikha, S. Photoactive graphene: Chemical functionalization using photosensitive functional group. *J. Optoelectron. Adv. Mater.* **2014**, *16*, 1170–1174.
126. Wang, H.-X.; Hao-Li, Z. Photoactive Graphene—From Functionalization to Applications. In *Graphene New Trends and Development*; InTech Open: London, UK, 2015. [CrossRef]
127. Maciel, E.V.S.; Mejía-Carmona, K.; Jordan-Sinisterra, M.; Da Silva, L.F.; Medina, D.A.V.; Lanças, F.M. The Current Role of Graphene-Based Nanomaterials in the Sample Preparation Arena. *Front. Chem.* **2020**, *8*, 664. [CrossRef] [PubMed]
128. Li, J.; Wang, L.; Dai, L.; Zhong, L.; Liu, B.; Ren, J.; Xu, Y. Synthesis and characterization of reinforced acrylate photosensitive resin by 2-hydroxyethyl methacrylate-functionalized graphene nanosheets for 3D printing. *J. Mater. Sci.* **2018**, *53*, 1874–1886. [CrossRef]
129. Palaganas, J.O.; Palaganas, N.B.; Ramos, L.J.I.; David, C.P.C. 3D Printing of Covalent Functionalized Graphene Oxide Nanocomposite via Stereolithography. *ACS Appl. Mater. Interfaces* **2019**, *11*, 46034–46043. [CrossRef] [PubMed]
130. de León, A.S.; de la Mata, M.; Delgado, F.J.; Molina, S.I. Printable Graphene Oxide Nanocomposites as Versatile Platforms for Immobilization of Functional Biomolecules. *Macromol. Mater. Eng.* **2022**, *307*, 2100784. [CrossRef]
131. Uysal, E.; Çakir, M.; Ekici, B. Graphene oxide/epoxy acrylate nanocomposite production via SLA and importance of graphene oxide surface modification for mechanical properties. *Rapid Prototyp. J.* **2021**, *27*, 682–691. [CrossRef]
132. Guo, B.; Ji, X.; Wang, W.; Chen, X.; Wang, P.; Wang, L.; Bai, J. Highly flexible, thermally stable, and static dissipative nanocomposite with reduced functionalized graphene oxide processed through 3D printing. *Compos. Part B Eng.* **2020**, *208*, 108598. [CrossRef]
133. Varma, M.V.; Kandasubramanian, B.; Ibrahim, S.M. 3D printed scaffolds for biomedical applications. *Mater. Chem. Phys.* **2020**, *255*, 123642. [CrossRef]
134. Weng, Z.; Zhou, Y.; Lin, W.; Senthil, T.; Wu, L. Structure-property relationship of nano enhanced stereolithography resin for desktop SLA 3D printer. *Compos. Part A Appl. Sci. Manuf.* **2016**, *88*, 234–242. [CrossRef]
135. Scalera, F.; Corcione, C.E.; Montagna, F.; Sannino, A.; Maffezzoli, A. Development and characterization of UV curable epoxy/hydroxyapatite suspensions for stereolithography applied to bone tissue engineering. *Ceram. Int.* **2014**, *40*, 15455–15462. [CrossRef]
136. Rouf, T.B.; Kokini, J.L. Biodegradable biopolymer–graphene nanocomposites. *J. Mater. Sci.* **2016**, *51*, 9915–9945. [CrossRef]
137. Kengla, C.; Kidiyoor, A.; Murphy, S.V. Chapter 68—Bioprinting Complex 3D Tissue and Organs. In *Kidney Transplantation, Bioengineering and Regeneration*; Orlando, G., Remuzzi, G., Williams, D.F., Eds.; Academic Press: Cambridge, MA, USA, 2017; pp. 957–971.
138. Song, X.; Zhang, Z.; Chen, Z.; Chen, Y. Porous Structure Fabrication Using a Stereolithography-Based Sugar Foaming Method. *J. Manuf. Sci. Eng.* **2016**, *139*, 031015. [CrossRef]
139. Bhanvadia, A.A.; Farley, R.T.; Noh, Y.; Nishida, T. High-resolution stereolithography using a static liquid constrained interface. *Commun. Mater.* **2021**, *2*, 41. [CrossRef]
140. Tumbleston, J.R.; Shirvanyants, D.; Ermoshkin, N.; Janusziewicz, R.; Johnson, A.R.; Kelly, D.; Chen, K.; Pinschmidt, R.; Rolland, J.P.; Ermoshkin, A.; et al. Continuous liquid interface production of 3D objects. *Science* **2015**, *347*, 1349–1352. [CrossRef] [PubMed]
141. De Beer, M.P.; Van der Laan, H.L.; Cole, M.A.; Whelan, R.J.; Burns, M.A.; Scott, T.F. Rapid, continuous additive manufacturing by volumetric polymerization inhibition patterning. *Sci. Adv.* **2019**, *5*, eaau8723. [CrossRef]
142. Bustillos, J.; Montero, D.; Nautiyal, P.; Loganathan, A.; Boesl, B.; Agarwal, A. Integration of graphene in poly(lactic) acid by 3D printing to develop creep and wear-resistant hierarchical nanocomposites. *Polym. Compos.* **2017**, *39*, 3877–3888. [CrossRef]
143. V-Niño, E.D.; Lantada, A.D.; Lonne, Q.; Durán, H.A.E.; Mejía-Ospino, E.; Ramírez-Caballero, G.; Endrino, J.L. Manufacturing of Polymeric Substrates with Copper Nanofillers through Laser Stereolithography Technique. *Polymers* **2018**, *10*, 1325. [CrossRef]

144. Andryushina, N.S.; Stroyuk, O.L.; Dudarenko, G.V.; Kuchmiy, S.Y.; Pokhodenko, V.D. Photopolymerization of acrylamide induced by colloidal graphene oxide. *J. Photochem. Photobiol. A Chem.* **2013**, *256*, 1–6. [CrossRef]
145. Sanchez-Rexach, E.; Johnston, T.G.; Jehanno, C.; Sardon, H.; Nelson, A. Sustainable Materials and Chemical Processes for Additive Manufacturing. *Chem. Mater.* **2020**, *32*, 7105–7119. [CrossRef]
146. Voet, V.S.D.; Strating, T.; Schnelting, G.H.M.; Dijkstra, P.; Tietema, M.; Xu, J.; Woortman, A.J.J.; Loos, K.; Jager, J.; Folkersma, R. Biobased Acrylate Photocurable Resin Formulation for Stereolithography 3D Printing. *ACS Omega* **2018**, *3*, 1403–1408. [CrossRef] [PubMed]
147. Chiappone, A.; Roppolo, I.; Naretto, E.; Fantino, E.; Calignano, F.; Sangermano, M.; Pirri, F. Study of graphene oxide-based 3D printable composites: Effect of the in situ reduction. *Compos. Part B Eng.* **2017**, *124*, 9–15. [CrossRef]
148. Liaw, C.-Y.; Guvendiren, M. Current and emerging applications of 3D printing in medicine. *Biofabrication* **2017**, *9*, 024102. [CrossRef] [PubMed]
149. Kim, S.; Bruyas, A.; Pan, C.-C.; Stahl, A.M.; Yand, Y. Vascularized Tissue Regenerative Engineering Using 3D Bioprinting Technology. In *Encyclopedia of Biomedical Engineering*; Narayan, R., Ed.; Elsevier: Oxford, UK, 2019; pp. 696–706. [CrossRef]
150. Achawi, S.; Pourchez, J.; Feneon, B.; Forest, V. Graphene-Based Materials In Vitro Toxicity and Their Structure–Activity Relationships: A Systematic Literature Review. *Chem. Res. Toxicol.* **2021**, *34*, 2003–2018. [CrossRef] [PubMed]
151. Wang, W.; Passarini, J.R., Jr.; Nalesso, P.R.L.; Musson, D.; Cornish, J.; Mendonça, F.; Caetano, G.F.; Bártolo, P. Engineered 3D printed poly(ε-caprolactone)/graphene scaffolds for bone tissue engineering. *Mater. Sci. Eng. C* **2019**, *100*, 759–770. [CrossRef] [PubMed]
152. Ma, Q.; Yang, L.; Jiang, Z.; Song, Q.; Xiao, M.; Zhang, D.; Ma, X.; Wen, T.; Cheng, G. Three-Dimensional Stiff Graphene Scaffold on Neural Stem Cells Behavior. *ACS Appl. Mater. Interfaces* **2016**, *8*, 34227–34233. [CrossRef]
153. Park, S.Y.; Park, J.; Sim, S.H.; Sung, M.G.; Kim, K.S.; Hong, B.H.; Hong, S. Enhanced Differentiation of Human Neural Stem Cells into Neurons on Graphene. *Adv. Mater.* **2011**, *23*, H263–H267. [CrossRef]
154. Yoon, H.H.; Bhang, S.H.; Kim, T.; Yu, T.; Hyeon, T.; Kim, B.-S. Dual Roles of Graphene Oxide in Chondrogenic Differentiation of Adult Stem Cells: Cell-Adhesion Substrate and Growth Factor-Delivery Carrier. *Adv. Funct. Mater.* **2014**, *24*, 6455–6464. [CrossRef]
155. Ku, S.H.; Park, C.B. Myoblast differentiation on graphene oxide. *Biomaterials* **2013**, *34*, 2017–2023. [CrossRef] [PubMed]
156. Nayak, T.R.; Andersen, H.; Makam, V.S.; Khaw, C.; Bae, S.; Xu, X.; Ee, P.L.R.; Ahn, J.-H.; Hong, B.H.; Pastorin, G.; et al. Graphene for Controlled and Accelerated Osteogenic Differentiation of Human Mesenchymal Stem Cells. *ACS Nano* **2011**, *5*, 4670–4678. [CrossRef]